Bi-stability resistant to fluctuations

M. Caruel [a,*], L. Truskinovsky [b]

[a] *Université Paris Est, Laboratoire Modélisation et Simulation Multi Echelle, MSME-UMR-CNRS-8208, 61 Avenue du Général de Gaulle, 94010 Créteil, France*
[b] *PMMH, CNRS UMR 7636, ESPCI, PSL, 10 rue de Vauquelin, 75231 Paris cedex 05, France*

A R T I C L E   I N F O

A B S T R A C T

We study a simple micro-mechanical device that does not lose its snap-through behavior in an environment dominated by fluctuations. The main idea is to have several degrees of freedom that can cooperatively resist the de-synchronizing effect of random perturbations. As an inspiration we use the power stroke machinery of skeletal muscles, which ensures at sub-micron scales and finite temperatures a swift recovery of an abruptly applied slack. In addition to hypersensitive response at finite temperatures, our prototypical Brownian snap spring also exhibits criticality at special values of parameters which is another potentially interesting property for micro-scale engineering applications.

© 2017 Elsevier Ltd. All rights reserved.

1. Introduction

Recent progress in micro and nano fabrication techniques opened new ways of building materials endowed with non-conventional mechanical properties (Cho et al., 2016; Florijn et al., 2014; Haghpanah et al., 2016; Nicolaou and Motter, 2012; Xin and Lu, 2016). A large class of such material can be viewed as multi-scale distributed mechanisms capable of internal switching transitions due to controllable micro instabilities. The applications of the materials-mechanisms with tunable multi-stability range from energy harvesting and acoustic cloaking to mechanical memory and tissue engineering (Bückmann et al., 2015; Frenzel et al., 2016; Halg, 1990; Harne and Wang, 2013; Harne, R L et al., 2016; Nadkarni et al., 2016; Paulose et al., 2015; Rafsanjani et al., 2015; Receveur et al., 2005).

Typical systems of this type require for their functioning mechanical elements with nonconvex elastic energy (Shan et al., 2015), but it is not obvious that such nonconvexity can be sustained at finite temperatures. In other words, it is not clear whether the discontinuous response of these elements can survive progressive miniaturization to scales where thermal [or non-thermal (Sheshka et al., 2016)] fluctuations cannot be neglected (Flood et al., 2004; Li and Gao, 2016; Ollier et al., 1995; Steuerman et al., 2004). This question is relevant because at sufficiently high temperatures mechanical barriers can be crossed uncontrollably causing the effective "disintegration" of the underlying snap-through mechanisms. Given that suppression of fluctuations at small scales may be either impossible, or too costly, special engineering solutions are needed that take advantage of the fluctuations without compromising the robustness of the switching.

In search of how to build a mechanical snap spring that preserves its hypersensitivity to loading in the presence of random fluctuations, we turn to biological systems which are known to operate with remarkable robustness in the Brownian environment. For instance, muscle contraction, hair cell gating, cell adhesion and neurotransmitter release, all involve fast

---

* Corresponding author.
  E-mail address: matthieu.caruel@u-pec.fr (M. Caruel).

conformational transitions which ensure their extremely sharp, almost digital (all-or-none) response to external mechanical stimulation (Howard and Hudspeth, 1988; Martin et al., 2000; Reconditi et al., 2004; Südhof, 2013). Even a superficial examination shows that all these systems employ the same basic design principle to fight the de-synchronizing effect of temperature.

Since a system with one degree of freedom cannot resist thermal rounding of its mechanical response (Shiino, 1987), a way to maintain multi-stability at elevated temperatures is to engage simultaneously many coupled degrees of freedom that can synchronize. To maintain the complexity of the energy landscape in a fluctuating environment one needs to ensure that the energy barriers separating different wells diverge with the system size. This can happen when a system develops macro-wells corresponding to synchronized configurations involving large number of elements and when individual elements can escape from such energy wells only cooperatively.

Biological examples suggest that this fundamental mechanism is ubiquitous in living systems. In inanimate world, similar idea is behind the functioning of ferromagnetic materials, where individual bi-stable elements (spins) behave cooperatively at low temperatures, allowing one to store non-mechanical information robustly. In such spatially extended systems, the switch takes place in the form of propagating domain walls. A zero dimensional macro-molecular mechanism with a cooperative behavior can still rely on interacting bi-stable elements but the local spin interactions would have to be replaced by the global interactions transmitted through sufficiently stiff backbones.

To show how such bio-mimetically inspired design idea can be implemented in engineering systems, we study in this paper the simplest mechanical example: a parallel bundle of snap springs loaded by a force. This toy model mimics the power stroke mechanism in acto-myosin contractile apparatus allowing a sub-micron muscle sarcomere to recover an abruptly applied slack at a time scale of 1 ms despite the exposure to a thermal bath and without any use of metabolic resources (ATP) (Caruel and Truskinovsky, 2016).

The abrupt transitions at finite temperatures become possible when the free energy (rather than elastic energy) is non-convex, and it is known in statistical mechanics that this can take place in macroscopic systems due to the presence of long-range interactions (Lebowitz and Penrose, 1966). For us, of particular interest in this respect are the zero dimensional systems with infinitely long range (mean-field) interactions (Desai and Zwanzig, 1978; Kometani and Shimizu, 1975). In the context of fast force recovery in skeletal muscles, a mean-field model was first proposed in the seminal paper by Huxley and Simmons (HS) (Caruel and Truskinovsky, 2016; Huxley and Simmons, 1971), where the authors considered a parallel bundle of bi-stable elements subjected to white noise. However, since the study of HS was performed in a hard device (length clamp) prohibiting collective effects, the cooperative behavior was not found. While the HS model has been since generalized (Caruel and Truskinovsky, 2016; Hill, 1974; 1976; Huxley and Tideswell, 1996; Linari et al., 2010; Piazzesi and Lombardi, 1995; Smith et al., 2008) and reformulated in the context of cell adhesion (Bell, 1978) and hair cell gating (Howard and Hudspeth, 1988), the issue of hypersensitivity of the mechanical response and the possibility of abrupt transitions at finite temperature in response to incremental loading have not been addressed.

In the present paper, we take advantage of the fact that the behavior of systems with long-range interactions is ensemble dependent (Barré et al., 2002) and study the distinctly different behavior of the HS model in the soft device conditions (load clamp). This seemingly innocent generalization of the original HS setting brings with it the desired mean-field elastic interactions that ensure that a parallel bundle of bi-stable units loaded by a force can maintain a synchronized state in the presence of thermal fluctuations.

Moreover we show that such mechanical system in a soft device can be mapped into a ferromagnetic Ising model with mean-field interactions, which is known to exhibits not only metastability abut also critical behavior at the particular values of parameters.

To substantiate this analogy, we present a systematic study of mechanical and thermal properties for a finite size HS model with a soft device loading. We show that for this mechanical system one can identify a critical temperature where both mechanical and thermal susceptibilities diverge. Below this temperature, the system is macroscopically bi-stable, exhibiting synchronized fluctuations between two coherent states. Given that the transitions between the two states are abrupt, such fluctuations can be viewed as a representation of domain structure in time (rather than space). Above the critical temperature, the non-equilibrium free energy of the system is convex with a minimum describing uncorrelated fluctuations and corresponding to "non-snap-spring" behavior. We show that the existence of a critical point can be already felt at finite N, and that the degree of synchronization can be tuned by varying the number of elements. In addition to equilibrium behavior, we study the kinetic response of the system, and show that sharp equilibrium transitions in quasi-static conditions give rise to hysteretic behavior at finite loading rates. The survival of the jumps inside the hysteresis loop emphasizes the robustness of the discontinuous behavior.

The paper is organized as follows. In Section 2, we analyze the behavior of a single element bi-stable system and conclude that in this case the abrupt response is always compromised by finite temperature. In Section 3, we study the finite temperature transition between synchronized and non-synchronized responses of a finite size cluster of interacting bi-stable elements. The properties of the critical point are detailed in Section 4. The kinetic behavior of cluster of snap-spring is studied in Section 5. Our results are summarized in Section 6. In the three Appendices A, B and C we briefly discuss the equilibrium susceptibility, the thermal behavior of the system and the limits of bi-stability.

In a companion paper (Caruel and Truskinovsky, 2016) we show that although the hard device version of the HS model does not exhibit a cooperative snap-through behavior, its mechanical response is characterized by an intriguing negative stiffness.
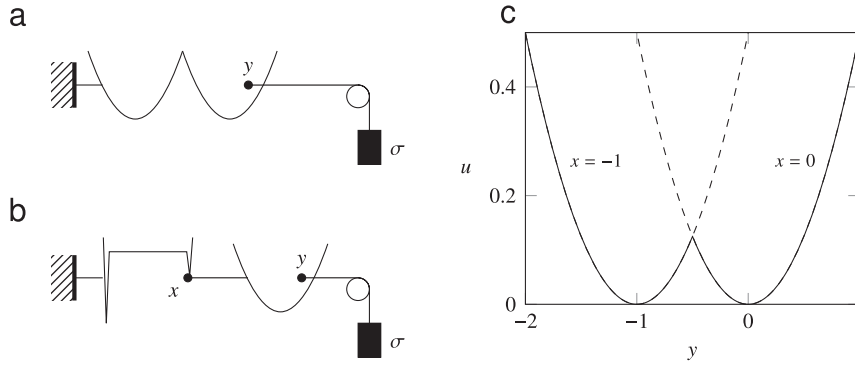
Fig. 1. Model of a single mechanical switch. (a) Snap-spring model; (b) Digital switch (spin) model. (c) Internal energy landscape of the device as function of its total elongation y; solid line, mechanical switch; dashed line, digital switch. Here $v_0 = 0$.

2. Single element

Consider a bistable spring with one degree of freedom y shown in Fig. 1(a). Its double-well energy, which for analytical transparency we choose to be bi-quadratic, can be written as

$$u(y) = (1/2)(|y + 1/2| - 1/2)^2,$$

see the solid line in Fig. 1(c). The system has two stable states located at $y = -1$ and $y = 0$, that are separated by an energy barrier located at $y = -1/2$.

Suppose that this device is submitted to an external force σ, so that the total energy of the system is $w(y) = u(y) - \sigma y$. In equilibrium, a metastable configuration must satisfy

$$(y + 1/2)[1 - 1/(2|y + 1/2|)] = \sigma,$$

which means, in particular, that at $\sigma = 0$, the system following the global minimum path will undergo a finite jump in y.

At a finite temperature T, the same system is described by the probability distribution

$$\rho(y, \beta) = Z^{-1} \exp[-\beta w(y; \sigma)],$$

where $\beta = 1/(k_b T)$, with k_b being Boltzmann's constant. From the partition function[1]

$$Z(\sigma, \beta) = \int_{-\infty}^{\infty} \exp[-\beta w(y; \sigma)]dy = \sqrt{\frac{\pi}{2\beta}} \left\{ \exp\left[-\beta\left(\sigma - \frac{\sigma^2}{2}\right)\right] \text{erfc}\left[\sqrt{\frac{\beta}{2}}\left(\sigma - \frac{1}{2}\right)\right] \right.$$
$$\left. + \exp\left[-\beta\left(-\frac{\sigma^2}{2}\right)\right] \text{erfc}\left[\sqrt{\frac{\beta}{2}}\left(\sigma + \frac{1}{2}\right)\right] \right\},$$

we obtain the equilibrium free energy

$$g(\sigma, \beta) = -\beta^{-1} \log[Z(\sigma, \beta)].$$

The constitutive relation linking the control parameter σ and the average elongation $\langle y \rangle$ takes the form

$$\langle y \rangle(\sigma; \beta) = -\frac{\partial}{\partial \sigma} g(\sigma, \beta) = \sigma - \left\{ 1 + \exp[\beta \sigma] \frac{\text{erfc}\left[-\sqrt{\beta/2}(\sigma + 1/2)\right]}{\text{erfc}\left[\sqrt{\beta/2}(\sigma - 1/2)\right]} \right\}^{-1}.$$

The resulting tension elongation relation is illustrated in Fig. 2(a). While at zero temperature (dashed line), the desired switch-like character of the response is clearly visible with an abrupt transition taking place at $\sigma = 0$, at any finite temperature (dotted and solid lines), the response is smooth.

To show that this result is independent on the detailed structure of the snap spring element, we now consider another representation of a bi-stable device (Huxley and Simmons, 1971). We introduce a spin variable x, and link it through a linear spring of stiffness κ_0 with a continuous variable y. The energy associated with the spin variable x is

$$u_0(x) = \begin{cases} v_0 & \text{if } x = 0 \\ 0 & \text{if } x = -a \\ \infty & \text{otherwise} \end{cases}$$

---

[1] Here we use the complementary error function $\text{erfc}(x) = \frac{2}{\sqrt{\pi}} \int_x^{\infty} \exp\left[-t^2\right]dt$.
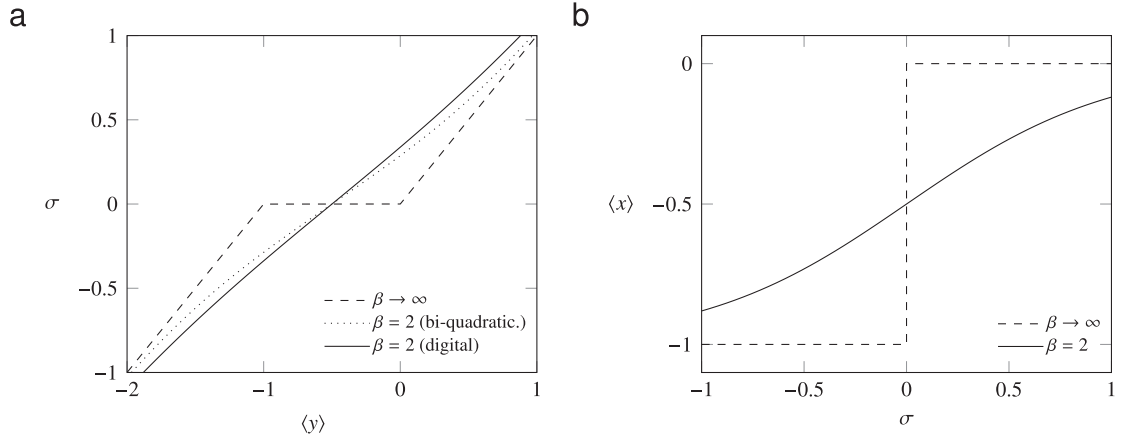
Fig. 2. Single switching element at finite temperature. (a) Average elongation as function of the applied load; At zero temperature ($\beta \to \infty$, dashed line), the response is the same with both the two models. At finite temperature ($\beta = 2$) the bi-quadratic (dotted) and the digital switch (solid) show similar smoothened responses. (b) Average internal configuration of the digital spin model at zero temperature (dashed line) and at finite temperature (solid line). Results are shown for $v_0 = 0$.

Here a is the "reference" length of the spin element, and v_0 is the intrinsic energy bias between the two states; see Fig. 1(b). We take a as our characteristic distance and $\kappa_0 a^2$ as the characteristic energy. Hence the non-dimensional energy of the spin element can be written as $u(x, y) = (1 + x)v_0 + (y - x)^2/2$, where now y represents the continuous total elongation while x takes the discrete values -1 or 0. At a given elongation, our element has two states $v_0 + y^2/2$ and $(y + 1)^2/2$, which are represented by dashed lines in Fig. 1(c). These two states have the same energy at

$$y = y_0 \equiv v_0 - 1/2.$$

Using dimensionless variables we can write the total energy of such system exposed to the force σ as

$$w(x, y; \sigma) = (1 + x)v_0 + (1/2)(y - x)^2 - \sigma y. \tag{1}$$

At zero temperature, we again obtain an abrupt transition. Indeed, if we minimize out the elongation y, the energy (1) takes the form

$$\hat{w}(x; \sigma) = -\frac{1}{2}\sigma^2 - \sigma x + (1 + x)v_0.$$

The global minimum of this energy correspond to $x = -1$ for $\sigma < \sigma_0$, and $x = 0$ for $\sigma > \sigma_0$, with the transition occurring at

$$\sigma = \sigma_0 \equiv v_0.$$

Therefore, for $v_0 = 0$, the digital switch element [Fig. 1(b)] and the snap spring element [Fig. 1(a)] behave similarly at zero temperature; see Fig. 2[(a), dashed line].

At finite temperature T, the spin device is described by the probability distribution

$$\rho(x, y; \sigma, \beta) = Z^{-1} \exp[-\beta w(x, y; \sigma)],$$

where the nondimensional measure of the thermal fluctuations is

$$\beta^{-1} = (k_b T)/(\kappa_0 a^2).$$

The partition function is given by

$$Z(\sigma, \beta) = \int_{-\infty}^{\infty} \sum_x \exp[-\beta w(x, y; \sigma)]dy = \sqrt{\frac{2\pi}{\beta}} \exp\left[-\frac{\beta}{2}(-\sigma^2 + \sigma + \sigma_0)\right] 2 \cosh\left[\frac{\beta}{2}(\sigma - \sigma_0)\right]. \tag{2}$$

The free energy then takes the form,

$$g(\sigma, \beta) = -\frac{\sigma^2}{2} + \frac{\sigma - \sigma_0}{2} + \sigma_0 - \frac{1}{\beta} \log\left\{2 \cosh\left[\frac{\beta}{2}(\sigma - \sigma_0)\right]\right\} - \frac{1}{2\beta} \log\left[\frac{2\pi}{\beta}\right],$$

while the relation between the control parameter σ and the average elongation $\langle y \rangle$ reads

$$\langle y \rangle(\sigma, \beta) = -\frac{\partial g}{\partial \sigma} = \sigma - \frac{1}{2} + \frac{1}{2} \tanh\left[\frac{\beta}{2}(\sigma - \sigma_0)\right].$$

As in the case of the snap spring device at finite temperature, the discontinuity at $\sigma = 0$ disappears. Since the difference between the two systems is only of quantitative nature, see Fig. 2[(a), dotted and solid lines], we abandon in what follows the soft spin description and focus exclusively on the digital switch model which is analytically more transparent.
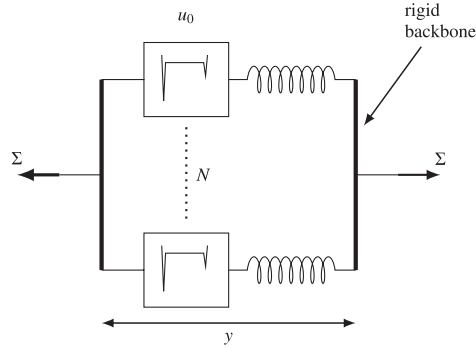
Fig. 3. Mechanical model of a cluster of N digital switches in parallel submitted to an external force Σ.

In addition to the total elongation, we have access to the average internal configuration of the spin element, which can be written as

$$\langle x \rangle (\sigma, \beta) = \sum_x \int x \rho(x, y; \sigma, \beta) dy = \langle y \rangle (\sigma, \beta) - \sigma = -\frac{1}{2}\left\{ 1 - \tanh\left[\frac{\beta}{2}(\sigma - \sigma_0)\right]\right\}.$$

The dependence of $\langle x \rangle$ on the applied force is shown in Fig. 2(b), for the case $v_0 = 0$. At zero temperature we observe the predicted discontinuity at $\sigma = 0$. At finite temperature the response loses its switch-like behavior: it is destroyed by thermal fluctuations because they allow the system to visit both spin states at fixed σ.

In Appendix A, we complement our analysis of a single element system by studying the behavior of its equilibrium *susceptibility* and a closely related elastic *stiffness*. In Appendix B, we discuss its *thermal* properties particularly focusing on the parametric dependence of the entropy and the specific heat.

3. Parallel bundle of N elements

To overcome the virtual "desintegration" of the switching device at finite temperature, we now consider N elements attached in parallel between two rigid backbones; see Fig. 3. The internal energy

$$v(\boldsymbol{x}; z) = \frac{1}{N}\sum_{i=1}^{N}\left[(1 + x_i)v_0 + \frac{1}{2}(y - x_i)^2 \right], \tag{3}$$

depends only on two non-dimensional parameters, v_0 and N. Here $\boldsymbol{x}$ denotes the vector $(x_1, \ldots, x_N)$. In a soft device setting (force clamp), we prescribe the total tension Σ, and the energy per element can be written as $w = v - \sigma y$, where $\sigma = \Sigma / N$. Note that a switch in a single unit has to be compensated by the changes in the other elements to ensure the force balance. This mechanical feedback can be characterized as a mean-field interaction.

At finite temperature, the probability density associated with a microstate $\boldsymbol{x}$ is given by

$$\rho(\boldsymbol{x}, y; \sigma, \beta) = Z(\sigma, \beta)^{-1}\exp\left[-\beta N w(\boldsymbol{x}, y; \sigma)\right],$$

where

$$Z(\sigma, \beta) = \int \sum_{\boldsymbol{x}\in\{0,1\}^N}\exp\left\{-\beta N[v(\boldsymbol{x}; y) - \sigma y]\right\}dy.$$

Due to the parallel connection, the system is invariant with respect to permutation of the variables x_i. Therefore the sum over the microstates can be transformed into a sum over

$$p = -\frac{1}{N}\sum_{i=1}^{N}x_i,$$

which represents the fraction of elements in the "short" phase. We thus obtain

$$Z(\sigma, \beta) = \int \sum_{Np=0}^{N}\binom{N}{Np}\exp\left\{-\beta N[\bar{v}(p, y) - \sigma y]\right\}dy, \tag{4}$$

where $\binom{N}{Np} = \frac{N!}{(Np)!(N-Np)!}$ is the degeneracy at a given value of p, and

$$\bar{v}(p; y, \beta) = p\frac{1}{2}(y + 1)^2 + (1 - p)\left[\frac{1}{2}y^2 + v_0\right], \tag{5}$$
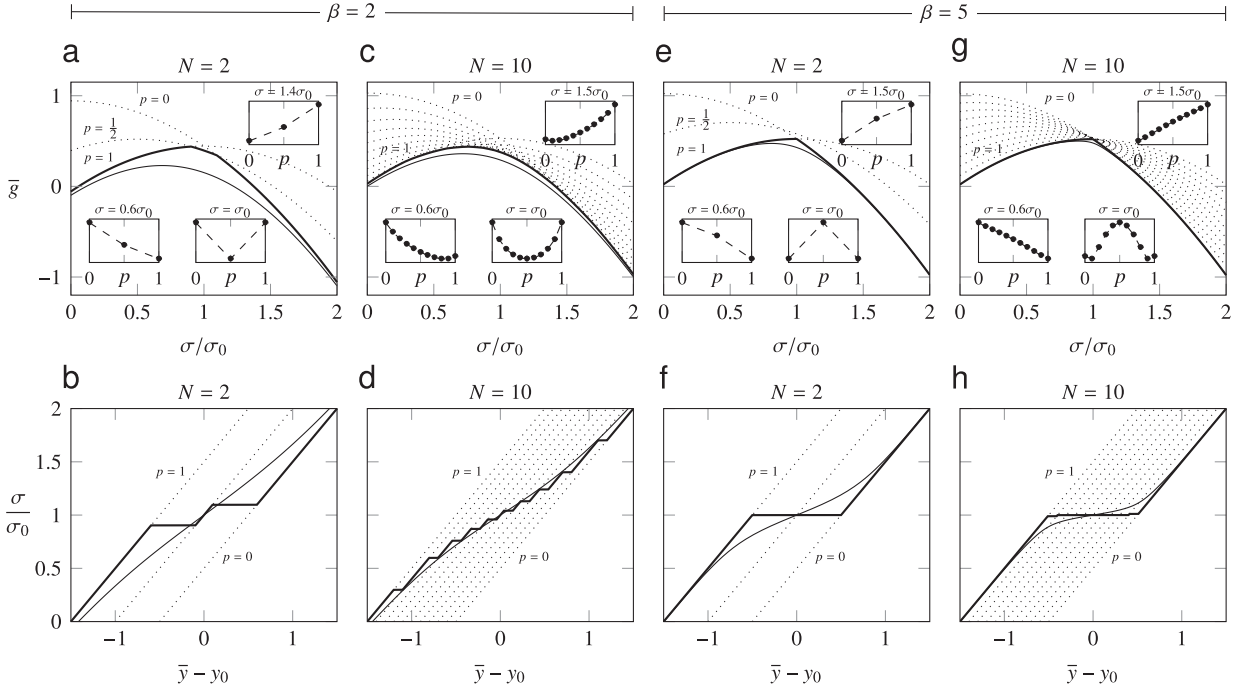
Fig. 4. Marginal free energy and tension-elongation of the HS model in a soft device at $\beta = 2$ [(a) to (d)] and $\beta = 5$ [(e) to (h)] for $N = 2$ [(a), (b) and (e), (f)] and for $N = 10$ [(c), (d) and (g), (h)]. First row, marginal free energy levels $\bar{g}$ corresponding to different values of p [dotted lines, see Eq. (8)], global minimum (bold line). Inserts show the free energy profiles for the selected values of the applied force. Second row, tension-elongation relations corresponding to each case of the first row with same line styles. In each plot, the thin solid line represents the behavior in thermal equilibrium.

is the internal energy of a metastable state at fixed (p, y). The partition function (4) can also be put in the form

$$Z(\sigma, \beta) = \int \sum_p \exp\left[-\beta N \bar{g}(p, y; \sigma, \beta)\right] dy \tag{6}$$

where $\bar{g}$ is the marginal free energy at fixed (p, y) defined by

$$\bar{g}(p, y; \sigma, \beta) = \bar{v}(p, y) - \sigma y - \frac{1}{\beta} s(p). \tag{7}$$

Here $\bar{v}$ is given by (5), and the entropy is

$$s(p) = \frac{1}{N} \log \binom{N}{Np}.$$

By integrating over y in (6), we obtain another marginal free energy

$$\bar{g}(p; \sigma, \beta) = \bar{w}(p, \sigma) - \frac{1}{\beta} s(p) - \frac{1}{2\beta N} \ln\left(\frac{2\pi}{\beta N}\right), \tag{8}$$

where,

$$\bar{w}(p; \sigma) = \sigma_0 - \frac{1}{2}\sigma^2 + p(\sigma - \sigma_0) + \frac{1}{2}p(1 - p), \tag{9}$$

is the mechanical energy of a metastable state characterized by p; see Caruel et al. (2015). We recall here that in our dimensionless variables $\sigma_0 = v_0$. The presence of the term $p(1 - p)$ in Eq. (9) can be viewed as the signature of interactions providing a mechanical coupling between the elements. To obtain the equilibrium value of the elongation, we minimize (7) with respect to y, and find $\bar{y} = \sigma - p$.

To illustrate these formulas, we note that in the case $N = 2$ [see Fig. 4(a), (b), (e) and (f)], the marginal free energy can only take one of the following values,

$$\bar{g}(0; \sigma, \beta) = -\frac{1}{2}\sigma^2 + v_0 + C(\beta),$$

$$\bar{g}(1/2; \sigma, \beta) = -\frac{1}{2}\sigma^2 + \frac{1}{2}\sigma + \frac{1}{8} + \frac{1}{2}v_0 + -\frac{1}{2\beta}\ln 2 + C(\beta), \tag{10}$$
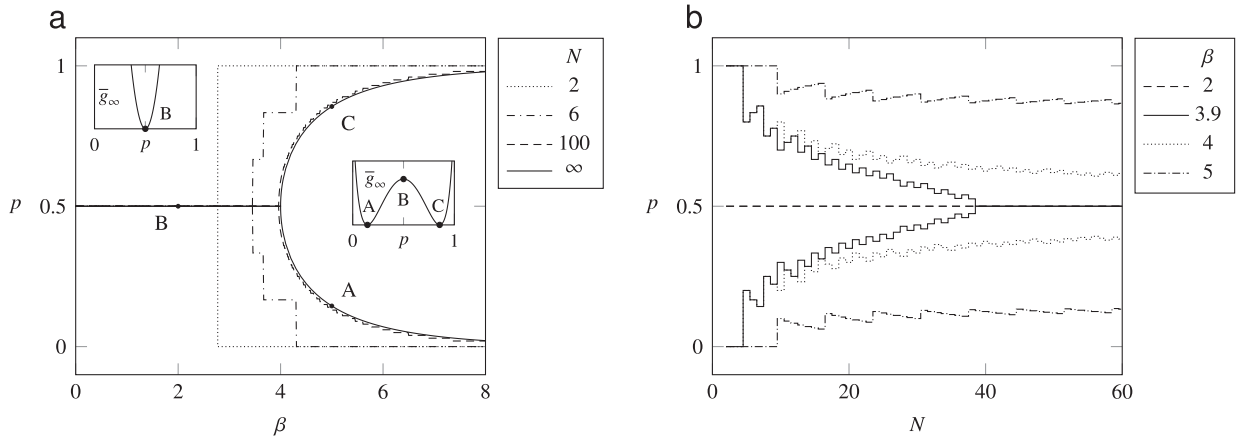
Fig. 5. Bifurcation diagrams at $\sigma = \sigma_0$, obtained by fixing the number of units and changing the temperature (a) and by fixing the temperature and changing the number of units (b). Each curve shows the local minima of the marginal free energy (8). The inserts in (a) show typical marginal free-energy profiles corresponding to sub- and supercritical temperatures in the thermodynamic limit.

$$\bar{g}(1; \sigma, \beta) = -\frac{1}{2}\sigma^2 + \sigma + C(\beta),$$

with $C(\beta) = -1/(4\beta) \ln[\pi/\beta]$. In Fig. 4 we present the energy profiles and the corresponding tension-elongation relations for systems with $N = 2, 10$ at $\beta = 2$, see Fig. 4[(a)–(d)]; and at $\beta = 5$; see Fig. 4[(e)–(h)]. For each value of σ, the metastable state with the lowest free energy gives a point on the global minimum path shown by the bold line. Note that above a certain temperature the free energy is a convex function of p (see inserts in Fig. 4[(a) and (c)]), which implies that the global minimum path goes through all mixed configuration with $0 \leq p \leq 1$. Below this temperature, the free energy is not convex (see inserts in Fig. 4[(e) and (g)]) and the mixed states may have higher energy than the ordered states. As a result, the system following (as σ increases or decreases) the global minimum path, will experience an abrupt jump between the almost homogeneous metastable configurations with $p \approx 0, 1$, while the mixed states are simply swept through. The resulting tension elongation curve will exhibit a plateau whose length indicates the size of the jump, see Fig. 4[(f) and (h)].

Even though the global minimization of the marginal energy does not describe the equilibrium behavior of the system, the above observations suggest that there is an order-disorder transition in the system (with pure states dominating at low temperatures, and mixed state dominating at high temperatures). For finite N, the parameters of the transition can be estimated by computing the discrete derivatives of the marginal free energy (8), which will converge to the derivatives of $\bar{g}$ in the thermodynamic limit. Thus, if we define the finite difference $\Delta^2 \bar{g} = \bar{g}(p + 1/N) + \bar{g}(p - 1/N) - 2\bar{g}(p)$ we obtain, for $N > 2$

$$N^2 \Delta^2 \bar{g}(p; \sigma, \beta) = -1 + \frac{N}{\beta} \log\left[1 + \frac{N+1}{N^2 p(1-p)}\right].$$

This expression is positive for $\beta < \beta_c$, with

$$\beta_c = N \log\left[1 + 4\frac{N+1}{N^2}\right],$$

and is negative otherwise. Hence, for $\beta < \beta_c$, the system has a single value of p minimizing (8), while for $\beta > \beta_c$ the same system is bistable. Similarly for a given value of β, we can find a critical size N_c below which the system becomes bistable. The positions of the minima of the marginal free energy (8) are represented in Fig. 5 as functions of the temperature [see (a)] and of the number of elements [see (b)] at the fixed value of the external force $\sigma = \sigma_0$.

Below the critical temperature ($\beta > \beta_c$), or below the critical system size ($N < N_c$), the marginal free energy has two minima corresponding to highly synchronized configurations. Notice that at this particular loading ($\sigma = \sigma_0$ and subcritical temperature $\beta > \beta_c$), the two minima of the free energy have the same depth (see the inserts of Fig. 4) and the free energy itself is symmetric independently of the choice of v_0. The size of the jump observed along the global minimum path corresponds in Fig. 5(a) to the distance between the two branches of the pitchfork bifurcation. When $N \to \infty$ the values of the critical temperature converge to $\beta_c = 4$, and Fig. 5(a) shows that this estimate is already adequate at $N = 100$ (see dashed line). Hence, it is possible to control the degree of synchronization by changing the cluster's size when $N \sim 10$. Above $N = 100$, the degree of synchronization does not depend anymore on the number of elements. These observations are summarized in the phase diagram shown in Fig. 6.

The formulas for the marginal free energy become more transparent in the thermodynamic limit $N \to \infty$ when we can use the Stirling formula $\log(n!) \approx n \log(n) - n$ and write the marginal free energy (7) as

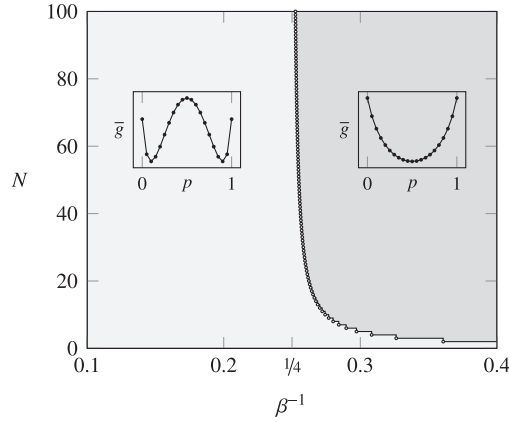$$\bar{g}_\infty(p, y; \sigma, \beta) = \bar{v}(y, p) - \sigma y - (1/\beta)s_\infty(p). \tag{11}$$

Fig. 6. Phase diagram for finite N, showing the domains where the system is cooperative (light gray) and noncooperative (dark gray). Inserts show typical marginal free energy profiles at $\sigma = \sigma_0$ in both phases.
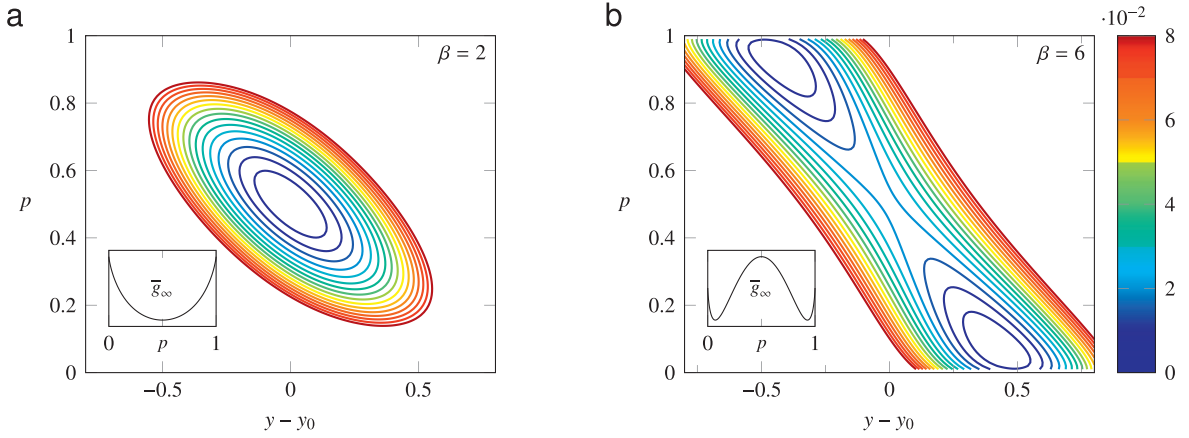

Fig. 7. Marginal free energy $\bar{g}_\infty$ at $\sigma = \sigma_0$ in the thermodynamic limit $N \to \infty$. (a) $\beta = 2$, (b) $\beta = 6$. The inserts show the energy profile of $\bar{g}_\infty$ after elimination of y. Energy minima are set to 0 for comparison and the contours associated to energy higher than 0.08 are not shown for the sake of clarity.

Here $s_\infty(p) = -[p \log(p) + (1-p) \log(1-p)]$, is the ideal mixing entropy. These formulas are illustrated in Fig. 7, where the level sets of the marginal free energy (11) are represented at $\sigma = \sigma_0$ for $\beta = 2$ [see (a)] and $\beta = 6$; see (b). We again see that the free energy is convex at large temperatures (a), and non-convex—with two macroscopic synchronized minima—at low temperatures (b). The critical temperature for this transition can be computed explicitly from the determinant of the Hessian matrix

$$H(p, \beta) = \begin{pmatrix} 1 & 1 \\ 1 & [\beta p(1-p)]^{-1} \end{pmatrix},$$

which is positive if $\beta < \min_{p \in [0,1]} [p(1-p)]^{-1} = \beta_c = 4$. The ensuing pitchfork bifurcation is represented by the solid line in Fig. 5(a).

The physical origin of the transition at β_c becomes more transparent if we introduce the new variable $\xi(p, y; \sigma) = y + p - \sigma$, and rewrite the free energy $\bar{g}_\infty$ as a function of ξ and p

$$\bar{g}_\infty(\xi, p; \sigma, \beta) = \frac{1}{2}\xi^2 + \overline{w}(p; \sigma) - \frac{1}{\beta} s_\infty(p), \tag{12}$$

where $\overline{w}$ is given by Eq. (9). We see that in Eq. (12) the function $\bar{g}_\infty$ is always convex in ξ. If we minimize out ξ, we obtain the one dimensional marginal free energy

$$\bar{g}_\infty(p; \sigma, \beta) = \overline{w}(p, \sigma) - \frac{1}{\beta} s_\infty(p). \tag{13}$$

Here the mechanical energy of the system $\overline{w}$ is always concave in p, implying that its minimum is reached at one of the two homogeneous states $p = 0$ or $p = 1$, while the mixed states are endowed with higher mechanical energy due to the mean-field interaction [manifested through the mixing energy $p(1-p)/2$ in Eq. (9)]. Instead, the entropy $s(p)$ is always convex
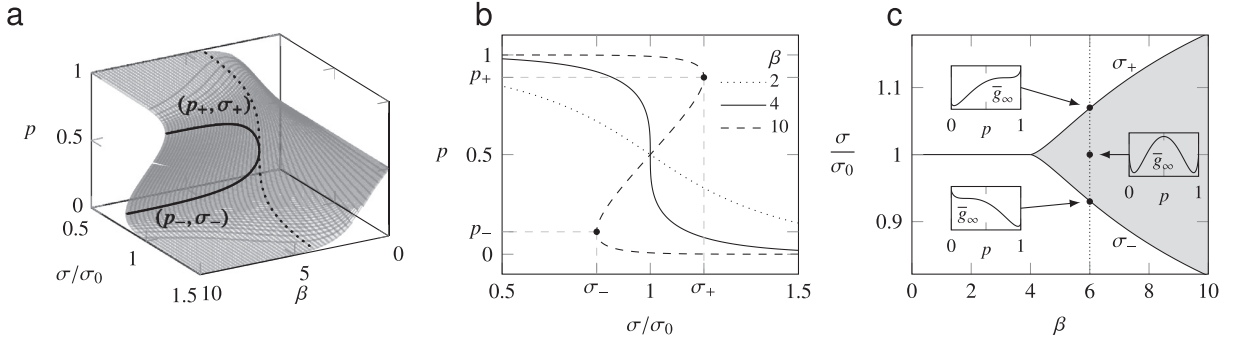
Fig. 8. Bistability domain. (a) Representation of the critical points of the marginal free energy $\bar{g}_\infty$ as function of temperature and loading. Dotted line, location of the minimum of the free energy $\bar{g}_\infty$ at the critical point $\beta = 4$; bold line, boundaries of the bistable domain. (b) Location of the minima of $\bar{g}_\infty$ for three different temperatures corresponding to three isotherms of (a). (c) Evolution of the bistable domain (gray area) delimited by the critical lines $\sigma_\pm$ as function of temperature. The inserts show the marginal free energy $\bar{g}_\infty$ for $\sigma = \sigma_\pm$ (left) and $\sigma = \sigma_0$ at $\beta = 6$.
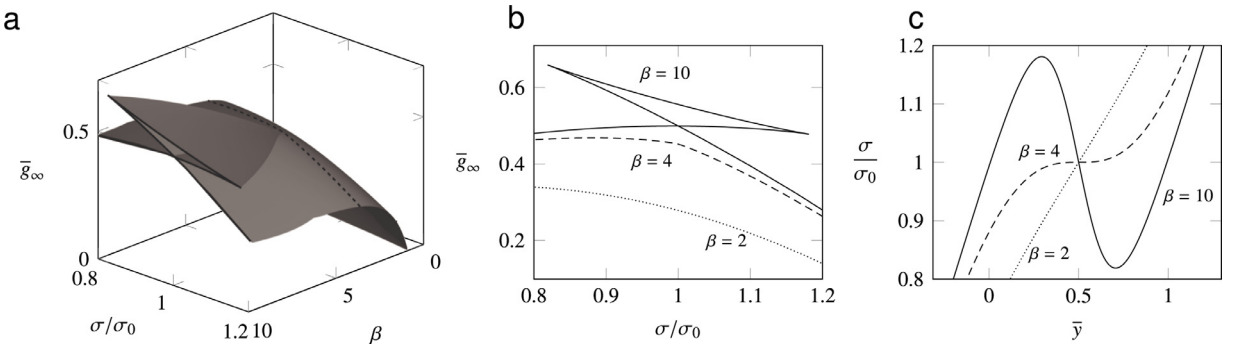

Fig. 9. Mechanical properties of the metastable states. (a) Marginal free energy shown as function of temperature and tension. For $\beta > 4$ (marked with the dotted line), and within the interval $[\sigma_-, \sigma_+]$, three energy levels coexist for the same tension. (b) Energy in the metastable states corresponding to three different temperatures (dotted, $\beta = 2$; dashed, $\beta = 4$; solid, $\beta = 10$). (c) Tension-elongation relations for the three same temperatures.

with a maximum at $p = 1/2$. Therefore the convexity of the free energy is an outcome of the competition between the term $p(1 - p)$ and the term $s_\infty(p)/\beta$, with the later becoming dominant at low β.

Energy profiles of $\bar{g}_\infty$ at $\sigma = \sigma_0$ are represented as function of p in the inserts of Fig. 7 for $\beta = 2$ [see (a)] and $\beta = 6$ [see (b)]. Above the critical point, the energy profile shows two metastable states that are illustrated in Fig. 8. Below the critical temperature, the domain of metastability spans the interval $[\sigma_-(\beta), \sigma_+(\beta)]$ whose boundary (derived explicitly in the thermodynamic limit in Appendix C) corresponds to a first order phase transition, see Fig. 8 [(b) and (c)]. The energies of the metastable states are shown in Fig. 9[(a) and (b)]. For each of these states, the elongation can be recovered from the relation $\bar{y}(p; \sigma, \beta) = \sigma - p$ obtained by adiabatic elimination of ξ in Eq. (12). Examples of such tension-elongation relations are shown in Fig. 9(c).

Using the marginal free energy $\bar{g}$ given by Eq. (8), we can rewrite the partition function (6) as

$$Z(\sigma, \beta) = \sum_p \exp\left[-\beta N \bar{g}(p; \sigma, \beta)\right], \tag{14}$$

and define the probability to find the equilibrium system in a particular metastable state

$$\bar{\rho}(p; \sigma, \beta) = Z^{-1}(\sigma, \beta) \exp\left[-\beta N \bar{g}(p; \sigma, \beta)\right]. \tag{15}$$

The average equilibrium configuration is then characterized by

$$\langle p \rangle(\sigma, \beta) = \sum_p p \, \bar{\rho}(p; \sigma, \beta).$$

In the thermodynamic limit, we can replace the sum in this expression by an integral over the interval [0, 1] and obtain $\langle p \rangle_\infty(\sigma, \beta) = p_*(\sigma, \beta)$, where p_* is the minimum of the marginal free energy $\bar{g}_\infty$, see Eq. (13). We have seen that the marginal free energy has two minima for $\beta > \beta_c = 4$. In the thermodynamic limit, the minimum with the lowest energy determines the equilibrium free energy and therefore, below the critical temperature the value of p_* jumps at $\sigma = \sigma_0$.

We illustrate the dependence of the average configuration on the loading in Fig. 10(a). Above the critical temperature ($\beta \leq 4$), the average configuration evolves smoothly between 1 and 0; while below it ($\beta > 4$), we observe an abrupt transition at $\sigma = \sigma_0$; see the thick line in Fig. 10(a). In Fig. 10[(c)–(e)], typical stochastic trajectories (with $N = 100$) of the order
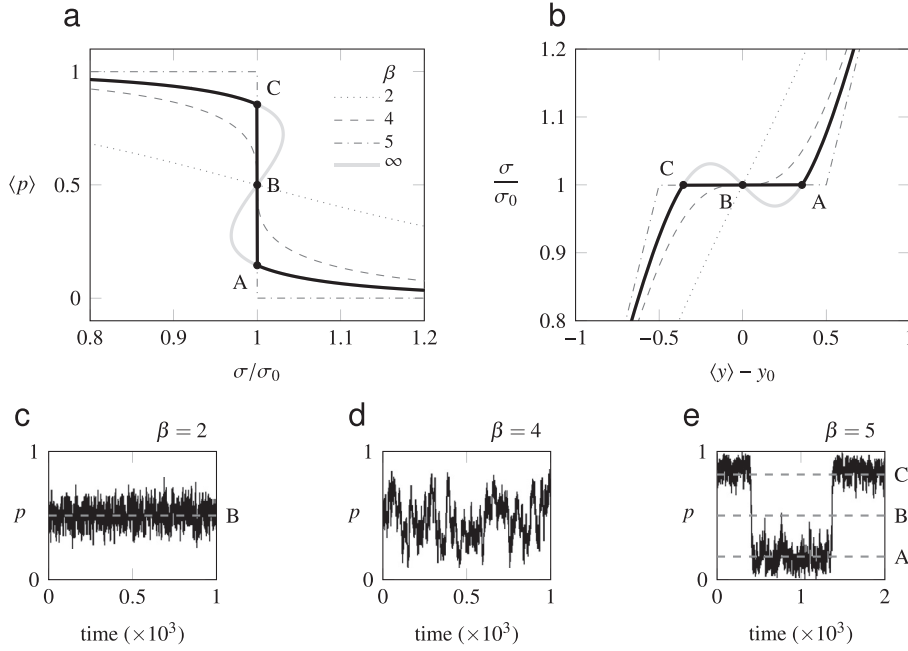
Fig. 10. Average internal configuration (a) and average elongation (b) obtained in the thermodynamic limit for several temperatures. In the case $\beta = 5$ (thick lines), we represent both the equilibrium curve (black) and the metastable states corresponding to the critical points of the marginal free energy (13) (gray). (c–e) Collective dynamics with $N = 100$ in a soft device under constant force $\sigma = \sigma_0$—ensuring $\langle p \rangle = 1/2$—for $\beta = 2$ (c), $\beta = 4$ (d) and $\beta = 5$ (e). The letters A, B and C label the different metastable states in the case $\beta = 5$.

parameter p are represented for different temperatures, where the tension $\sigma = \sigma_0$ is fixed to ensure that $\langle p \rangle = 1/2$. One can see that in the high temperature (paramagnetic) state [see Fig. 10(c)] the elements are in random conformations and the system fluctuate around the average value $p = 1/2$ (labeled B), corresponding to the single minimum of the free free energy; see Fig. 8[(a) and (b)]. Instead, in the low temperature (ferromagnetic) state [see Fig. 10(e)], the average value $p = 1/2$ corresponds to a local maximum of the free energy, which is an unstable state. As we illustrate in Fig. 10(e), thermal equilibrium in this regime is ensured by coherent fluctuations of the system between two synchronized states (labeled A and C).

We recall that in classical ferromagnetism, the average value of the magnetization, say $p = 1/2$, is ensured by the formation of spacial domain structure within the material. In our case of zero dimensional (mean-field) system, the spacial microstructure is replaced by a *temporal microstructure* formed by rare jumps between two coherent and long-living ordered configurations with $p \approx 1$ or $p \approx 0$. The time between the jumps is much larger than the characteristic time of the fluctuations near the metastable states. One can say that our switching device is endowed with a limited "mechanical memory" which is erased when the observation time (or loading time) exceeds the lifetime of the metastable states.

The mechanical properties of the equilibrium system can be obtained from the knowledge of the partition function (14). The equilibrium free energy at finite N takes the form

$$G(\sigma, \beta) = -\frac{1}{\beta} \log \left\{ \sum_p \exp\left[-\beta N \bar{g}(p; \sigma, \beta) \right] \right\},$$

see the thin lines in Fig. 4(first row). The equilibrium tension-elongation relation is obtained by differentiating the free energy with respect to the loading Σ,

$$\langle y \rangle (\sigma, \beta) = -\frac{\partial}{\partial \Sigma} G(\sigma, \beta) = \sigma - \langle p \rangle (\sigma, \beta). \tag{16}$$

The resulting tension-elongation relations are shown for different system sizes in Fig. 4(second row, thin lines).

To address the thermodynamic limit we introduce the equilibrium free energy per cross-linker, $g = G/N$. When $N \to \infty$, we can use Laplace method to obtain

$$g(\sigma, \beta)_\infty = \bar{g}_\infty[p_*(\sigma, \beta); \sigma, \beta],$$

where p_* has been defined above as the minimum of $\bar{g}_\infty$ at a given σ. In the same limit we obtain $\langle y \rangle (\sigma, \beta) = y_*(\sigma, \beta)$, where $y_* = \sigma - p_*$ is the solution of $\sigma(y, \beta) - \sigma = 0$ with

$$\sigma(y, \beta) = y + \frac{1}{2} \left\{ 1 - \tanh\left[\frac{\beta}{2}(y - y_0) \right] \right\}.$$

The equilibrium tension-elongation relations are illustrated in Fig. 10(b). These curves are monotone when $\beta \leq 4$, while for $\beta > 4$, they exhibit a plateau that extends as temperature decreases. In the limit $\beta \to \infty$, we recover the equilibrium response of the purely mechanical system corresponding to the global minimum path. The three points A, B and C represent the three solutions of $\sigma(y, \beta) = \sigma_0$: the system switches collectively between the fully synchronized configurations A and C. The transformation at the microscale associated with such switches translates into a large length change, whose amplitude is easily detectable even in the presence of thermally induced fluctuations. The device is then able to deliver a strong mechanical output in response to small load perturbations.

The behavior of the equilibrium *stiffness* of a parallel bundle of switching elements is discussed in Appendix A. In Appendix B we study the *thermal* properties of this system and show that below the critical temperature, not only isothermal but also adiabatic response of this Brownian snap spring is abrupt, and is accompanied by a substantial heat release in response to small variations of the external force.

4. Critical behavior

We have shown in the previous section that above the critical temperature our switching elements are completely desynchronized. This leads to a smooth mechanical response while the snap spring property is lost. Instead, below the critical temperature, the system can sustain thermal fluctuations and preserve its bistability. The latter can be then viewed as a cooperative effect.

At the critical point $\beta = 4$, $\sigma = \sigma_0$, the system has a degenerate energy landscape with a marginally stable minimum corresponding to the configuration with $p = 1/2$; see Fig. 10[(a) dashed line]. Near the critical point we obtain the expansions $p \sim 1/2 \pm (\sqrt{3}/4)[\beta - 4]^{1/2}$, for $\sigma = \sigma_0$, and $p \sim 1/2 - \text{sign}[\sigma - \sigma_0][(3/4)|\sigma - \sigma_0|]^{1/3}$, for $\beta = 4$. Both critical exponents take the classical (Landau) values characteristic of the mean field Ising model, see Balian (2006). These results suggest that small deviations from the critical point lead to significant changes in the configuration of the system. In Appendix A, we study the behavior of thermal and mechanical susceptibilities and show they reach their maximal values at $\sigma = \sigma_0$ and diverge at the critical point, see Fig. A.21.

Near the critical point we can write $\langle y \rangle - y_0 = \pm (\sqrt{3}/4)[\beta - 4]^{1/2}$, for $\sigma = \sigma_0$, and $\langle y \rangle - y_0 = \text{sign}[\sigma - \sigma_0][(3/4)|\sigma - \sigma_0|]^{1/3}$, for $\beta = 4$. The latter relation suggests that in critical conditions the tension-elongation curve has a plateau; see dashed line in Fig. 10(b). The corresponding stiffness is equal to 0 , see Appendix A, which means that upon application of a small positive (respectively negative) force increment, the system rapidly unfolds (respectively folds). Note that, below the critical temperature, similar behavior becomes irreversible, *i.e* depending on the position on the hysteresis loop the system can respond abruptly to either increase or a decrease of the external force. Characteristically, near the critical point both large elongation and large shortening can take place, which makes our system very reactive and versatile.

5. Rate dependent behavior

5.1. Single element

In some regimes the isothermal kinetics of a single switching element can be modeled using the Kramers approximation, which stipulates that the transition rate between two states depends primarily on the energy barrier separating these states. An expression of the energy barrier can be obtained by generalizing the original HS model. To this end we define a transitional state $x = \ell \in [-1, 0]$, between the unfolded ($x = 0$) and the folded ($x = -1$) configurations, characterized by the energy $v_* > v_0$, see Fig. 11 cf. Bormuth et al. (2014). In a soft device the kinetic response of a single element under fixed load σ includes the discrete jumps associated with x, and the continuous dynamics of y. We assume for simplicity that the viscous relaxation timescale associated with the elongation described by the variable y is negligible, which implies that y can be adiabatically eliminated and replaced by its equilibrium value at a given σ, namely $y = \bar{y} = \sigma + x$. This assumption can be of course relaxed if we endow the variable y with the appropriate Langevin dynamics.

In this simplified framework, we introduce the chemical rate constants describing the load-dependent kinetics of the direct and reverse transitions

$$\mathbb{P}(x^{t+dt} = -1 \,|\, x^t = 0) = k_+(\sigma, \beta)\, dt,$$
$$\mathbb{P}(x^{t+dt} = 0 \,|\, x^t = -1) = k_-(\sigma, \beta)\, dt,$$

where both k_+ and k_- depend on the loading σ and temperature β. By taking into account the elastic element, the energy barriers for the forward and the reverse transition can be written as

$$\Delta u_+(\sigma, \beta) = v_* - \ell\sigma - v_0,$$
$$\Delta u_-(\sigma, \beta) = v_* - \ell\sigma - \sigma,$$

and the corresponding transition rates are

$$k_+(\sigma, \beta) = (1/\tau)\exp[\beta(\ell\sigma + \sigma_0)],$$
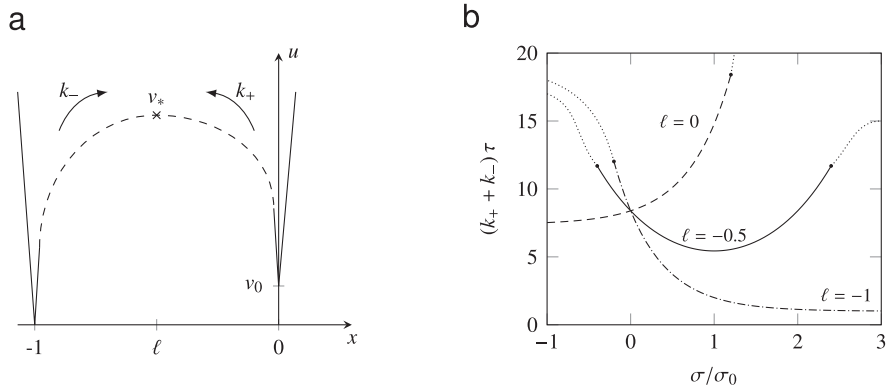$$k_-(\sigma, \beta) = (1/\tau)\exp[\beta(\ell\sigma + \sigma)],$$

(17)

Fig. 11. (a) Generalization of the Huxley and Simmons model of the energy barriers involving a transition state v_* corresponding to the conformation ℓ. (b) Equilibration rate between the states as function of the loading parameter at different values of ℓ. In (b) $v_0 = 1$, $v_* = 1.2$ and $\beta = 2$. Dotted constructions show a schematic representation of diffusion (*vs.* reaction) dominated processes.
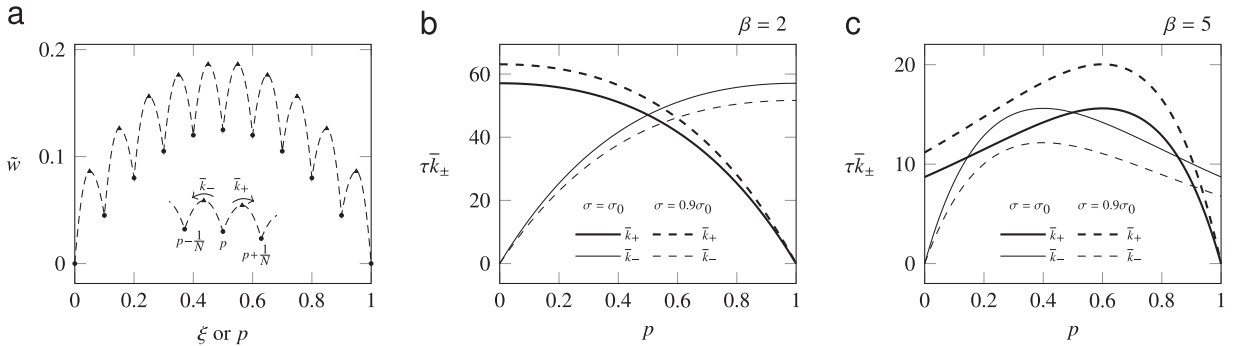

Fig. 12. Kinetic model for a parallel bundle of N elements. (a) Energy landscape characterizing the sequential folding process of $N = 10$ bistable elements at $\sigma = \sigma_0$. [(b) and (c)] Transition rates represented for $\sigma = \sigma_0$ (solid lines) and $\sigma = 0.9\sigma_0$ (dashed lines) at $\beta = 2$ (b) and $\beta = 5$ (c). Parameters are $v_0 = 1$, $v_* = 1.2$, and $\ell = -0.5$. In (a) $\beta = 2$.

where $1/\tau = \alpha \exp[-\beta v_*]$, with $\alpha = $ const., determines the timescale of the response. Notice that the above expressions are valid if Δu_+ and Δu_- are positive *i.e.* for $(v_* - v_0)/\ell < \sigma < v_*/(\ell + 1)$. Beyond this interval the Kramers description of the kinetics is no more valid and the dynamic response is controlled by the diffusive relaxation of the variables x, so one can expect a saturation at large loads, see Bell and Terentjev (2017). In the rest of the section, we only consider the situation where Eq. (17) is valid. In their original paper, HS worked in a particular setting where $\ell = -1$ which implies that $k_- = $ const. and $k_+(\sigma, \beta) = k_- \exp[-\beta(\sigma - \sigma_0)]$.

The equilibration rate $k_+ + k_-$ is represented as a function of the normalized load σ/σ_0 in Fig. 11(b). In the two limit cases $\ell = 0$ and -1, this rate is monotone and converges to constant value when $y \to \pm\infty$. In the case $\ell = -1$ considered by HS, the rate is a decreasing function of the load, see Fig. 11(b), dash-dotted line. This conclusion has been challenged by recent experimental data showing a nonmonotone dependence of the rate on the load, which supports the present generalization of the HS model, see Fig. 11(b), solid line and Offer and Ranatunga (2016). Moreover, the new experimental data show a saturation of the equilibration rate at large loads, which corroborates the fact that Kramers description is restricted to a finite interval of loads beyond which the dynamics is controlled by diffusion, see the dotted lines illustrating this saturation in Fig. 11(b).

5.2. Parallel bundle of N elements

5.2.1. Kinetic model

To characterize the transition rates in a cluster of $N > 1$ elements under fixed external force, we introduce the energy $\tilde{w}(p, p_*)$ corresponding to a configuration where p elements are folded ($x_i = -1$) and p_* elements are at the transition state ($x_i = \ell$). The "energy landscape" separating two configurations p and q can then be expressed in terms of the "reaction coordinate" $\xi = p - x(q - p)$, see Fig. 12(a).

The transition rates between neighboring metastable states are controlled by the energy barriers $\Delta w_+(\sigma) = \tilde{w}(p, 1/N; \sigma) - \overline{w}(p; \sigma)$ and $\Delta w_- = \tilde{w}(p - 1/N, 1/N; \sigma) - \overline{w}(p; \sigma)$, where $\overline{w}$ is defined by Eq. (9). We have

$$N\Delta w_+(p; \sigma) = \nu_* - \ell(\sigma - p) - \sigma_0 + (1 + 3/N)(\ell^2/2)$$

$$N\Delta w_-(p; \sigma) = \nu_* - (\ell + 1)(\sigma - p) + (1 + 3/N)(\ell^2/2) - (1 + N + 2\ell)/(2N)$$

which shows that the barriers corresponding to individual transitions are of the order of $1/N$ and therefore vanish in the thermodynamic limit; see a more detailed discussion of the energy barriers in Caruel et al. (2015).

By taking into account the degeneracy of the metastable states, we obtain that the ensuing one-dimensional random walk process is characterized by the transition probabilities

$$\mathbb{P}\left[p^{t+dt} = p^t + 1/N\right] = \overline{k}_+(p^t; \sigma, \beta)\, dt,$$
$$\mathbb{P}\left[p^{t+dt} = p^t - 1/N\right] = \overline{k}_-(p^t; \sigma, \beta)\, dt, \tag{18}$$
$$\mathbb{P}\left[p^{t+dt} = p^t\right] = 1 - \mathbb{P}\left[p^{t+dt} = p^t + 1/N\right] - \mathbb{P}\left[p^{t+dt} = p^t - 1/N\right],$$

where

$$\tau\, \overline{k}_+(p; \sigma, \beta) = N(1 - p)\exp\left\{-\beta\left[-\ell(\sigma - p) - \sigma_0 + (1 + 3/N)(\ell^2/2)\right]\right\},$$
$$\tau\, \overline{k}_-(p; \sigma, \beta) = N p \exp\left\{-\beta\left[-(\ell + 1)(\sigma - p) + (1 + 3/N)(\ell^2/2) - (1 + N + 2\ell)/(2N)\right]\right\}. \tag{19}$$

Behind the construction of this Markov chain is the assumption that only one element can switch within the interval $[t, t + dt]$. This assumption is reasonable as one can show that the energy barriers corresponding to several switching elements $(p_* > 1/N)$ are larger than the barrier involving only one shifting element.

The nondimensional rates (19) are represented in Fig. 12[(b) and (c)] for two different loading conditions, and two different temperatures. Notice that in Eq. (19), the prefactor and the exponential term have opposite tendencies in terms of p. At large temperatures $(\beta \to 0)$ the entropic prefactor dominates and the rates are monotone functions of p, see Fig. 12(b). At low temperatures, the exponential terms become non-negligible and the rate dependence on p looses monotonicity, see Fig. 12(c).

The mechanical coupling appearing in the exponent of (19) makes the dynamics non-linear. We recall that in the original HS model the dependence of the transition rates on p was linear because the cross-bridges were viewed as independent. The master equation describing the evolution of the probability density (omitting the dependence on σ and β for clarity) reads,

$$\frac{\partial}{\partial t}\overline{\rho}(p, t) = \overline{k}_+(p - 1/N)\overline{\rho}(p - 1/N, t) + \overline{k}_-(p + 1/N)\overline{\rho}(p + 1/N, t) - \left[\overline{k}_+(p) + \overline{k}_-(p)\right]\overline{\rho}(p, t). \tag{20}$$

The time independent equilibrium distribution, which can be obtained explicitly as a steady state solution $\overline{\rho}_{eq}$ of Eq. (20), takes the form (van Kampen, 2001)

$$\overline{\rho}_{eq}(p) = \frac{\prod_{Ni=1}^{Np} \frac{\overline{k}_+(i - 1/N)}{\overline{k}_-(i)}}{1 + \sum_{Nj=0}^{N}\prod_{Ni=0}^{Nj} \frac{\overline{k}_+(i - 1/N)}{\overline{k}_-(i)}}.$$

Using the definitions (19), we obtain after simplifications $\overline{\rho}_{eq}(p; \sigma, \beta) = Z(\sigma, \beta)^{-1}\exp\left[-\beta N \overline{g}(p; \sigma, \beta)\right]$, which is in agreement with Eq. (15).

5.2.2. First passage times and equilibration rates

To understand the peculiarities of the time dependent response of the parallel bundle of N elements, it is instructive to first derive the expression for the mean first passage time $\tau(p \to p')$ characterizing transition between two metastable states with Np and Np' ($p < p'$, the analysis in the case $p > p'$ is similar) switched elements. Assume a reflective boundary condition at $p = 0$ and an absorbing boundary condition at p'. Following Gardiner (2004) and omitting again the dependence on σ and β, we write

$$\tau(p \to p') = \sum_{Nk=Np}^{Np'} \left[\overline{\rho}(k)\overline{k}_+(k)\right]^{-1} \sum_{Ni=0}^{Nk} \overline{\rho}(i), \tag{21}$$

where $\overline{\rho}$ is the marginal equilibrium distribution at fixed p given by Eq. (15), and $\overline{k}_+$ is the forward rate (19).

In the case $\beta > \beta_c$ for the interval of loading $[\sigma_-, \sigma_+]$, the marginal free energy $\overline{g}$ has two minima which we denote $p = p_1$ and $p = p_0$, with $p_0 < p_1$. The minima are separated by a maximum located at $p = \hat{p}$.

We first illustrate the relaxation rate inside one of the macroscopic wells by establishing a reflective boundary condition at $p = \hat{p}$. The average rates $\overline{k}(\hat{p} \to p_{1,0}) = 1/\tau(\hat{p} \to p_{0,1})$ of reaching the metastable states ($p = 0$ or $p = 1$) starting from the top of the energy barrier $\hat{p}$ are represented as functions of the load in Fig. 13. These rates are almost constant over the entire interval of existence of the metastable states $[\sigma_-, \sigma_+]$. The rise at the boundaries is due to the proximity of the
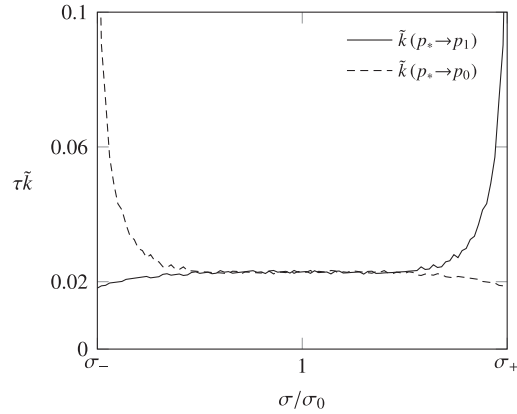
Fig. 13. Characteristic rate of relaxation to the metastable state in the case of a reflecting barrier at $p = \hat{p}$. The parameters are $N = 200$, $\beta = 5$ and $\ell = -0.5$.
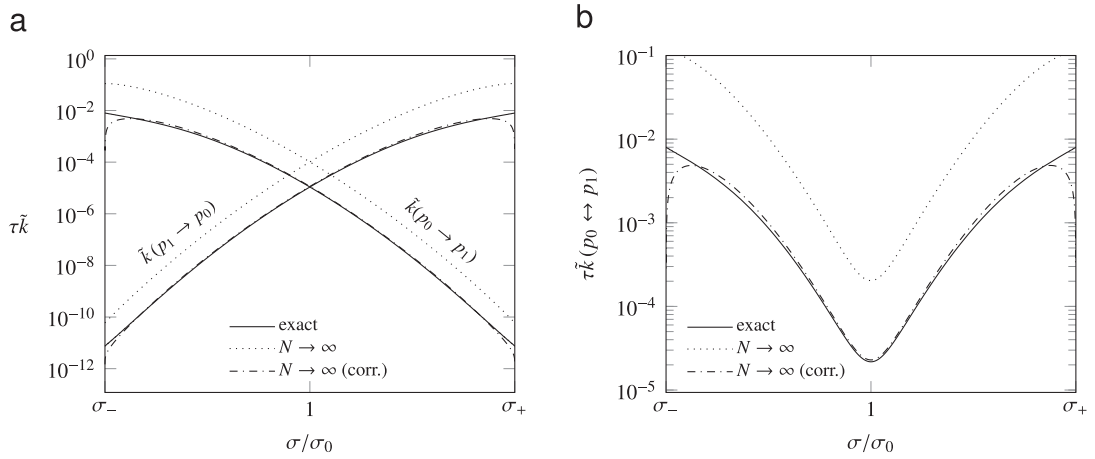

Fig. 14. Transition rates between the two macroscopic configurations $p_0(\sigma)$ and $p_1(\sigma)$. (a) Forward $[\tilde{k}(p_0 \to p_1)]$ and reverse $[\tilde{k}(p_1 \to p_0)]$ rates. (b) Equilibration rate $\tilde{k}(p_0 \leftrightarrow p_1) = \tilde{k}(p_0 \to p_1) + \tilde{k}(p_1 \to p_0)$. Solid line, exact computation from Eq. (21); dotted line, thermodynamic limit approximation given by Eq. (23); dot-dashed line, thermodynamic limit with corrected free energy. Parameters are the same as in Fig. 13.

barrier to the bottom of the energy well. From Fig. 13 we conclude, for instance, that for $N = 200$ and $\beta = 5$, the timescale of the internal relaxation is of the order of 10^{-2}.

If we now consider the transition between the two macrostates, Eq. (21) can be simplified when N is sufficiently large. In this case, the sums in Eq. (21) can be transformed into integrals

$$\tau(p_0 \to p_1) = N^2 \int_{u=p_0}^{p_1} \left[\overline{\rho}(u)\overline{k}_+(u)\right]^{-1} \left[\int_0^u \overline{\rho}(v)dv\right] du. \tag{22}$$

The inner integral in Eq. (22) can be computed using Laplace method and noticing that the function $\overline{g}$ has a single minimum in the interval $[0, u > p_0]$ located at p_0, we obtain

$$\tau(p_0 \to p_1) = \sqrt{2\pi N} \left[\beta \left|\overline{g}''(p_0)\right|\right]^{-\frac{1}{2}} \int_{u=p_0}^{p_1} \left[\overline{\rho}(u)\overline{k}_+(u)\right]^{-1} \overline{\rho}(p_0)du.$$

In the remaining integral, the inverse density $(1/\overline{\rho})$ is sharply peaked at $p = \hat{p}$ so again using Laplace method we can write

$$\tau(p_0 \to p_1) = 2\pi(N/\beta)\overline{k}_+(\hat{p})^{-1} \left|\overline{g}''(p_0)\overline{g}''(\hat{p})\right|^{-\frac{1}{2}} \exp\left\{\beta N\left[\overline{g}^\infty(\hat{p}) - \overline{g}^\infty(p_0)\right]\right\}, \tag{23}$$

The rates $\tilde{k}(p_{0,1} \to p_{1,0}) = \left[\tau(p_{0,1} \to p_{1,0})\right]^{-1}$ corresponding to the forward $(p_0 \to p_1)$ and reverse $(p_1 \to p_0)$ collective transitions are represented in Fig. 14(a) as functions of the loading $\sigma \in [\sigma_-, \sigma_+]$ for $N = 200$. The presence of the barrier considerably slowers the transition process comparing to the simple relaxation process illustrated in Fig. 13. However, the order of magnitude (10^{-2}) of the simple relaxation process is recovered at the boundaries of the interval $[\sigma_-, \sigma_+]$.

The comparison of the intrabassin relaxation (see Fig. 13) and the interbassin transition (see Fig. 14) shows that the system has now two characteristic timescales. The first one depends on the micro energy barriers between neighboring micro-configurations and scales with τ. The second timescale is of the order of $\exp[N\Delta\bar{g}]$ [see Eq. (23)], where $\Delta\bar{g}$ is the height of the macroscopic energy barrier separating the two metastable states. In the thermodynamic limit, this energy barrier grows linearly with N, which prevents collective *interbasin* dynamics and generates metastability: glass like "freezing" in one of the two globally coherent configurations.

Note that in Fig. 14 there is a non-negligible quantitative difference between the exact result based on Eq. (21)(solid line) and the asymptotic formulas derived in Eq. (23) (dotted line). This difference may be explained by the fact that even though the microscopic barriers vanish in the thermodynamic limit, the dynamics cannot be straightforwardly reduced to a diffusion process on the smooth potential $\bar{g}_\infty$. The presence of at least two scales in the kinetics requires a more subtle asymptotic description, see for instance Zwanzig (1988).

One can refine the analytical results by considering a finer approximation of the entropy in the thermodynamic limit. In Eq. (11), the ideal mixing entropy $s_\infty = -p\log(p) - (1-p)\log(1-p)$ is obtained from the Stirling formula $\log(n!) = n\log(n) - n + O[\log(n)]$. A finer approximation consists in writing $\log(n!) = n\log(n) - n + (1/2)\log(2\pi n) + O(1/n)$, which leads to $s_\infty = -(p + \frac{1}{2N})\log(p) - (1 - p + \frac{1}{2N})\log(1-p) - \frac{1}{2N}\log(2\pi N)$. By Using the latter expression for the entropy in the definition of the marginal free energy (13) we can obtain a better quantitative agreement between the exact and the approximated rates, see dot-dashed lines in Fig. 14. The above computations suggest that the equilibration rate between the two macrostates [see Fig. 14(b)] decreases exponentially in the vicinity of $\sigma = \sigma_0$ while increasing for both $\sigma > \sigma_0$ and $\sigma < \sigma_0$. This contradicts the non symmetric behavior of the transition rate predicted in Huxley and Simmons (1971) where the symmetry was broken due to the assumption $\ell = -1$. Our more general results for $-1 \leq \ell \leq 0$ are supported by the recent experiments reported in Offer and Ranatunga (2016).

5.2.3. Coarse grained dynamics

The simplest approach to solving Eq. (20) is focusing exclusively on the dynamics of averages. To this end we may multiply Eq. (20) by p and sum the result over p. We then obtain a kinetic equation

$$N\frac{\partial}{\partial t}\langle p \rangle = \langle \bar{k}_+(p) \rangle - \langle \bar{k}_-(p) \rangle. \tag{24}$$

To close this model we need to use the mean-field type approximation giving us the (nonlinear) analog of the chemical reaction equation of HS; see Huxley and Simmons (1971). By noticing that the rate functions are convex in p we can expand them around $\langle p \rangle$ to obtain,

$$\langle \bar{k}_\pm(p) \rangle = \bar{k}_\pm(\langle p \rangle) + \frac{1}{2}\langle [p - \langle p \rangle]^2 \rangle \frac{\partial^2 \bar{k}_\pm}{\partial p^2}\bigg|_{\langle p \rangle} + o\big\{\langle [p - \langle p \rangle]^2 \rangle\big\}.$$

In the thermodynamic limit, the fluctuations can be neglected and the kinetic Eq. (24) takes the mean-field form

$$N\frac{\partial}{\partial t}\langle p \rangle = \bar{k}_+(\langle p \rangle) - \bar{k}_-(\langle p \rangle). \tag{25}$$

In Appendix A, we show that close to the critical point we have the divergence $\langle [p - \langle p \rangle]^2 \rangle \sim [\beta - 4]^{-1}$, which limits the applicability of the approximate Eq. (25).

To follow the evolution of the variable $\langle y \rangle(t)$ in response to a prescribed loading protocol $\sigma(t)$, we can use the equilibrium relation $\langle y \rangle = \sigma - \langle p \rangle$ to obtain $\dot{\langle y \rangle} = \dot{\sigma} + (1/N)\big(\bar{k}_-(\sigma - \langle y \rangle) - \bar{k}_+(\sigma - \langle y \rangle)\big)$. The steady state solution of (25) can be then computed as a root of the transcendental equation

$$\langle p \rangle_\infty = \frac{1}{2}\left\{1 - \tanh\left[\frac{\beta}{2}\Big(\sigma - \sigma_0 - \langle p \rangle_\infty + \frac{1}{2}\Big)\right]\right\}.$$

5.2.4. Numerical illustrations

As a first illustration of the obtained relations, we consider behavior of the system with $N = 100$ elements subjected to slow increase of force from the value $0.5\,\sigma_0$ to the value $1.5\,\sigma_0$ in the time interval $[0, 1000\,\tau]$; see Fig. 15. The trajectories were obtained using a simple first order Euler numerical scheme simulation of the Markov process (18), with a time step equal to $10^{-3}\tau$. Average trajectories and distributions were obtained by numerically solving Eq. (20) with an explicit algorithm, which involved the computation of the transition matrix at each time step.

At supercritical temperatures [see (a) and (b)], the transition between the two states is smooth and can be described as a drift of a uni-modal probability density, which means that the system is fluctuating around a single mixed configuration with a time dependent average.

Below the critical point, the response shows hysteresis; see Fig. 15 [(c) and (d)]. This phenomenon is due to the presence of the macroscopic wells in the marginal free energy $\bar{g}$. The distribution of the elements inside the hysteresis domain $[\sigma_-, \sigma_+]$ becomes bi-modal and the escape time [see Eq. (23)], characterizing the equilibration between the two wells grows as $\exp[N]$. This prevent the equilibrium transition expected at $\sigma = \sigma_0$ to take place at the time scale of the loading. The collective switch is observed only when the energy barrier becomes of the order of 1, *i.e.* when the loading parameter reaches the boundary of the bi-stable interval $[\sigma_-, \sigma_+]$.
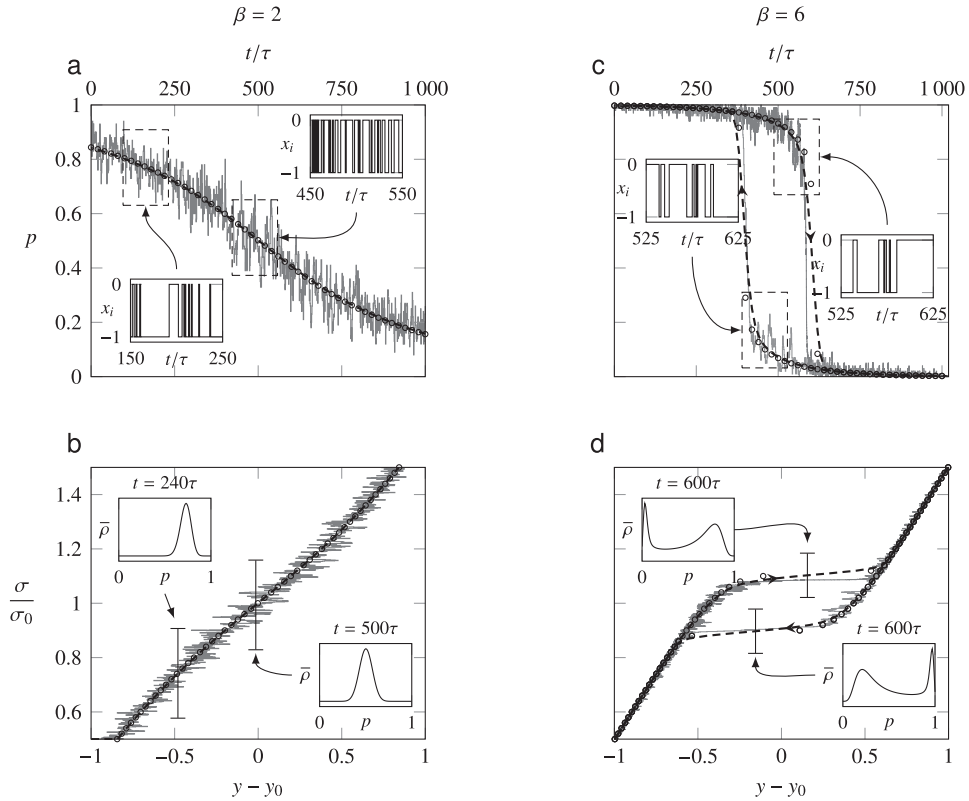
Fig. 15. Stochastic response to a quasi-static tension ramp imposed on a system with $N = 100$ and $\beta = 2$ (a,b) or $\beta = 6$ (c,d). In (a) and (b), the loading consists in a tension ramp from $0.5\sigma_0$ to $1.5\sigma_0$ achieved within $10^3\tau$. In (c) and (d), two trajectories are shown corresponding to two ramps, one from $0.5\sigma_0$ to $1.5\sigma_0$ and the other from $1.5\sigma_0$ to $0.5\sigma_0$. (a) and (c) Stochastic evolution [obtained from Eq. (18)] of the fraction of folded snap springs (gray) together with averages computed from the simulation of the master Eq. (20) (dashed lines). (b) and (d) Trajectories (gray) and corresponding averages (dashed lines) in the (y, σ) space. The inserts show samples of the trajectory of a single element corresponding to different time windows [(a) and (c)] and snapshots of the probability density $\bar{\rho}$ obtained from the numerical simulation of (20) [(b) and (d)]. Open symbols, responses obtained using the mean-field kinetic Eq. (25).

We note that the average trajectory is captured rather well by both, the master Eq. (20) and the mean-field kinetic Eq. (25), even in the presence of the hysteresis loop. This is due to the fact that the loading is sufficiently slow and the system remains close to the quasi-stationary states describing coherent metastable configurations.

As a second illustration of the general theory, we now consider the kinetics of the relaxation of the system submitted to an instantaneous force drop. This process would mimic to the so-called phase 2 of the fast transient shortening observed in skeletal muscle fibers under force-clamp loading protocols (Reconditi et al., 2004).

We first show in Fig. 16 sample trajectories obtained for different values of the force drop at two different temperatures, $\beta = 2$ [see (a)], and $\beta = 6$; see (b). For $\beta = 2$, the system is initiated in the configuration $p = 0.5$, and the load is dropped at $t = 0$ from σ_0 to $0.5\sigma_0$ (low value) or $0.8\sigma_0$ (high value). For $\beta = 6$ [see Fig. 16(b)], the system is initiated either at $p = 0.8$ (gray trace) or at $p = 0.1$ (black traces) and the load is dropped at $t = 0$ from $\sigma = \sigma_0$ to $0.5\sigma_0$, $0.8\sigma_0$ or $0.9\sigma_0$.

First of all, for both temperatures tested, we see that the larger the step size, the faster the response. At $\beta = 6$, there are two metastable states for $\sigma = \sigma_0$, the first one with $p \approx 0.1$ and the second one with $p \approx 0.9$. When the load is changed from $\sigma = \sigma_0$ to $\sigma = 0.9\sigma_0$, there is only one remaining state with $p \approx 1$. If the system is prepared in the well with local minimum at $p = 0.9$ [see gray trace in Fig. 16(b) obtained with the initial condition $p = 0.8$], it relaxes to the final state $p \sim 1$, without crossing any macroscopic barrier and in this respect the response is analog to the case where the system is not bistable *i.e.* it is characterized by only one timescale; see Fig. 16(a). However, if the system is prepared in the metastable with $p = 0.1$, the response contains two phases; see the trace with $\sigma = 0.9\sigma_0$ in Fig. 16(b). The first phase of the relaxation is slower than the second phase, and corresponds to the escape of the system from its initial metastable state. The second phase corresponds to the relaxation inside the final coherent state, which occurs without crossing any macroscopic barrier.

To illustrate further the quick relaxation process we now compare the average response obtained in the same loading conditions by using either the master Eq. (20), or the mean-field kinetic approximation (25); see Fig. 17. We observe that the kinetic slowing down induced by the collective effects in the case of high load, remains visible at low temperature: the corresponding probability distributions at different times are illustrated in Fig. 17(d–f). Remarkably, the mean-field approx-
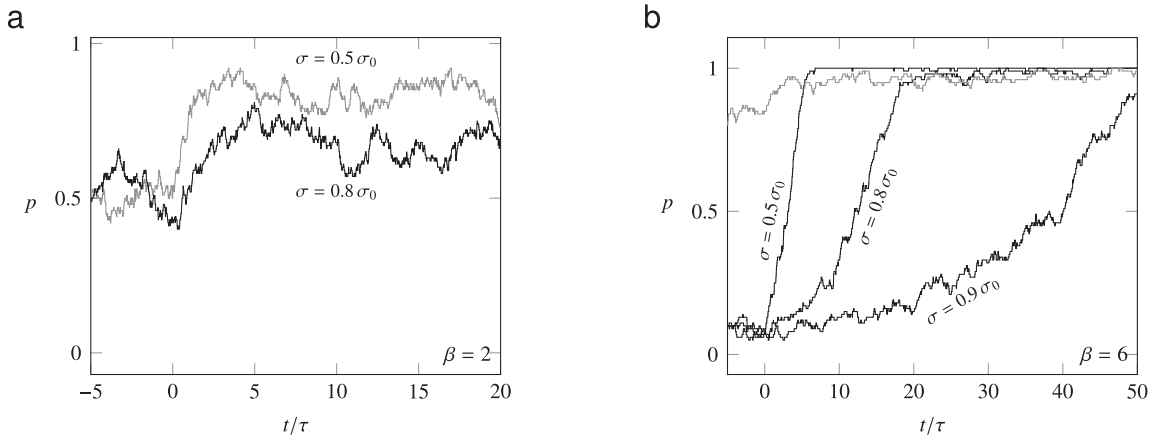
Fig. 16. Trajectories obtained when submitting the system to an instantaneous tension drop applied at $t = 0$ with $\beta = 2$ (a) or $\beta = 6$ (b). The initial tension is set to $\sigma = \sigma_0$ and the different curves correspond to different tension step sizes. In (b) the initial state of the system is set at $p = 0.1$ which corresponds to one of the macroscopic wells. The gray trace in (b) shows a single trajectory starting from the second macroscopic well ($p = 0.8$) for the case $\sigma = 0.9\sigma_0$.
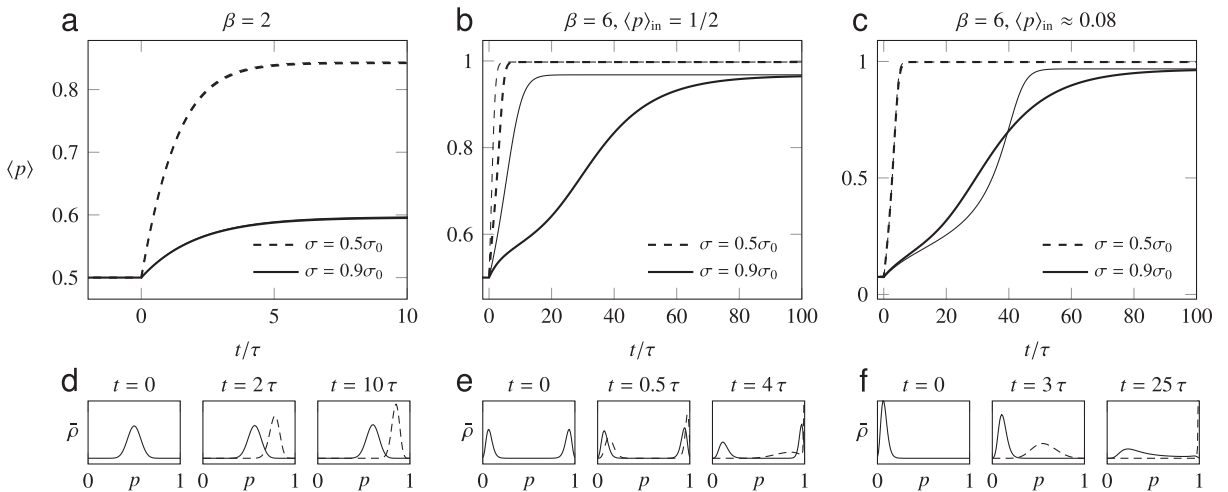
Fig. 17. Relaxation of the average conformation in response to fast force drops applied at $t = 0$ with $\beta = 2$ (a) and $\beta = 6$ [(b) and (c)]. Imposed forces after the step are equal to $0.5\sigma_0$ (dashed), and $0.9\sigma_0$ (solid). Thick lines, solutions from the master Eq. (20); thin lines, solutions from the mean-field dynamic Eq. (25). In (b), the initial condition corresponds to thermal equilibrium: bi-modal distribution and $\langle p \rangle_{in} = 1/2$. In (c), the initial condition corresponds to the unfolded metastable state: uni-modal distribution and $\langle p \rangle_{in} \approx 0.08$. Snapshots at different times of the probability density profiles corresponding to [(a)–(c)] are shown in [(d)–(f)], respectively.

imation is accurate at large temperatures [see thin lines in Fig. 17(a)] while it fails to reproduce the exact dynamics at low temperatures, even though the final equilibrium states are similar.

The observed difference between the chemo-mechanical description and the simulations targeting the full probability distribution is due to the fact that for the mean-field kinetics the transition rates are computed based on the average values of the order parameter. At large temperatures, where the distribution is uni-modal, the average value indeed correspond to the most probable state and therefore the mean-field kinetic theory captures rather-well the timescale of the response; see Fig. 17 (a). Instead, at low temperatures, since the equilibrium distribution is bi-modal, the average value corresponds to a state which is very poorly populated. The value of the order parameter that actually makes the kinetics slow corresponds to a metastable states and because of this discrepancy the mean-field kinetic equation fails to reproduce the real dynamics of the system; see Fig. 17[(b) and (e)].

Our results should not be interpreted in the sense that the mean-field approximation (25) fails to capture the two-stage relaxation process. We have just shown that at low temperatures it takes a long time for the system to reach the bi-modal equilibrium distribution and to acquire the associated equilibrium average. If instead the system is initially prepared in one of the metastable configurations but with the average order parameter different from the corresponding equilibrium value, the mean-field kinetics will capture correctly the two timescales of the response; see Fig. 17(c).
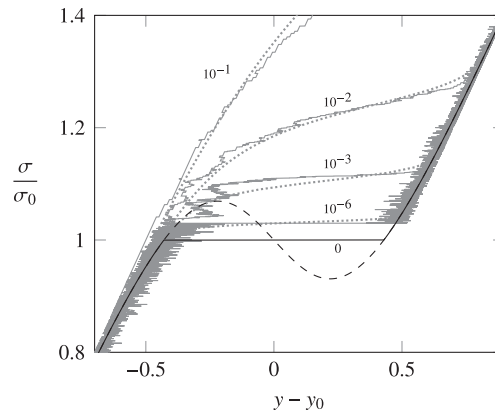
Fig. 18. Response of the system to ramp loading at different rates σ_0/τ (indicated by numbers besides each trace). Gray lines, stochastic trajectories (solid) shown together with average obtained from the master equation (dotted); black lines, metastable states (dashed) and equilibrium tension-elongation relation (thick solid). Parameters are $N = 100$ and $\beta = 6$.

To further illustrate the kinetics of the system, we study next the dependence of the response on the rate of loading, see Fig. 18. We vary the tension protocols in a broad range by changing the loading rate from $10^{-6}\sigma_0/\tau$ to $10^{-1}\sigma_0/\tau$. In the limit of slow driving $\sigma_0/\tau_0 \rightarrow 0$, the system can explore the whole phase space and therefore exhibits the equilibrium response, see solid black line in Fig. 18. At faster loading rates ($\sigma_0/\tau = 10^{-3}$ of 10^{-6}) the metastability becomes an issue and the system develops hysteresis bounded by the spinodal states. In these regimes the system remains trapped in the metastable states (dashed line) and the dynamics is dominated by interbasin kinetics, while only rare jumps between the metastable configurations are observed. This behavior is exaggerated as we decrease the temperature. Finally, sufficiently fast loading ($\sigma_0/\tau = 10^{-1}$ or 10^{-2}) drives the system away from the energy wells and the slowing down due to metastability becomes unimportant. In these regimes, the energy landscape changes faster than the individual unfolding events and the hysteresis becomes largely controlled by the intrabasin relaxation time.

Interestingly, quite similar behavior is exhibited by a chain of bistable elements connected in series, see Achenbach et al. (1986), Efendiev and Truskinovsky (2010), Benichou and Givli (2015) and Benichou et al. (2016). A recent work suggests that the kinetics of successive switching events in such systems may be controlled by a single parameter linking the rate of loading and the rate of internal relaxation (Benichou and Givli, 2015; Benichou et al., 2016). Similar data collapse can be expected to hold in the case of a parallel bundle of the HS type.

Our study of the kinetic properties of the model shows that the system has a mechanical memory due to the long escape time from a metastable state. When perturbed, it exhibits a relaxation rate that depends on the amplitude of the loading. The switch-like behavior characterized by a large mechanical output in response to small variations in external stress is then associated with a slow recovery phase. Its presence generates an effective damping which contributes to the robustness of the response in the presence of perturbations.

6. Conclusions

The fact that a single mechanical snap spring loses its discontinuous response in the presence of random perturbations becomes an important issue for the engineering devices employing bi-stability at nm scales. Behind the problem of building a "brownian snap spring" is the general problem of maintaining multi-stability in a fluctuating environment. An almost naive solution of this problem, proposed in the present paper, is to use a parallel cluster of N snap springs. Despite its simplicity, this mechanical toy, exhibits a rich class of equilibrium mechanical behaviors including abrupt transitions and criticality. Our study of kinetics shows that even though the rate effects may interfere with the ability of the system to undergo abrupt changes, such kinetic smoothening takes place at the time scale of the transition itself and if the controls are varied at the time scale which is larger than the fast transition time, the temperature itself cannot prevent such device from undergoing quasi-discontinuous transitions that are now embedded into a hysteresis loop.

Our analysis helps to understand why the presence of long-range interactions in this system is crucial for the preservation of bi-stability and ensuring razor-edge response at finite temperatures. We show that the ultra-sensitivity is achieved due to synchronization of strongly interacting individual snap springs. The dependence of the critical temperature on the number of elements N suggests that the transition from synchronized to de-synchronized behavior can be controlled by the system size. At the critical point, the mechanical response of the system is characterized by a zero stiffness which makes it anomalously responsive to external perturbations. This property is highly desirable in applications because it allows the system to amplify interactions and ensure strong feedback.

The prototypical device studied in the paper can serve as a mechanical memory unit resistant to random perturbations. The underlying macroscopic collective transition has a strong thermal signature which reveals itself in a substantial heat

release in response to the variation of the external force. This property could be useful for energy harvesting applications at the nanoscale. Another collective effect is the critical slowing down near the critical point which can be used in the design of adaptive dampers. The plethora of other applications for systems with bistable elements connected in parallel is discussed in Wu et al. (2016; 2014).

Acknowledgments

Appendix A. Susceptibility

In this Appendix we discuss the parametric dependence of the equilibrium susceptibility and stiffness in the case of a single switching element, and in the case of a parallel bundle of *N* such elements.

We begin with the behavior of a single element discussed in Section 2. The sensitivity of the system to changes in the external loading is characterized by the "susceptibility"

$$\chi(\sigma, \beta) = \frac{\partial}{\partial \sigma} \langle x \rangle (\sigma, \beta) = \beta \langle [x - \langle x \rangle (\sigma, \beta)]^2 \rangle, \tag{A.1}$$

where $\langle [x - \langle x \rangle (\sigma, \beta)]^2 \rangle = (1/4)\text{sech}[(\beta/2)(\sigma - \sigma_0)]^2$, is the variance of *x*. As in the case of a hard device [see Caruel and Truskinovsky (2016)], the susceptibility is maximum for $\sigma = \sigma_0$ [see Fig. A.19(a)], and becomes infinite in the zero temperature limit, due to the presence of a jump; see Fig. 2(b). For other values of applied force, the susceptibility is equal to zero both at zero temperature, when the system is "frozen" in one of the states, and at infinite temperature, when the mixing due to fluctuations dominates the bias introduced by the external force. Interestingly, it reaches a maximum at a finite value of β; see Fig. A.19(b). The susceptibility (A.1) is of interest because it is directly linked to the equilibrium stiffness

$$\kappa(\sigma, \beta) = \left[\frac{\partial \langle y \rangle}{\partial \sigma} \right]^{-1} = [1 + \chi(\sigma, \beta)]^{-1} > 0.$$

which has the Cauchy-Born and the fluctuations induced contributions; the only difference with the behavior in a hard device (Caruel and Truskinovsky, 2016) is that the fluctuation part comes with plus sign, which makes the stiffness always positive.

The equilibrium stiffness κ is represented as function of the external force and the temperature in Fig. A.20. Note that for $\beta \gg 1$, the stiffness decreases with temperature (softening) while for $\beta \to 0$, it increases (hardening). The major difference with the hard device behavior occurs at $\sigma = \sigma_0$, where the susceptibility becomes infinite, which makes the stiffness decreasing toward 0 (instead of $-\infty$ in a hard device) in the limit $\beta \to \infty$.

Next we move to the discussion of the system of *N* switching elements. First, we compute the equilibrium susceptibility

$$X(\sigma, \beta) = -\frac{1}{N} \frac{\partial}{\partial \sigma} \langle p \rangle (\sigma, \beta) = \beta \langle [p - \langle p \rangle (\sigma, \beta)]^2 \rangle \geq 0. \tag{A.2}$$
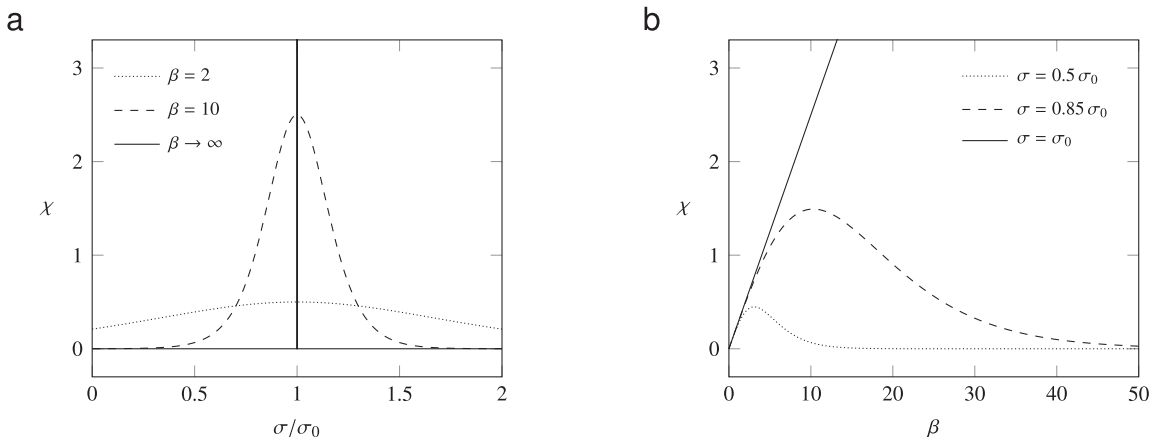
a

b

Fig. A.19. Susceptibility of a single digital switch represented as function of the loading (a), and as function of temperature (b).
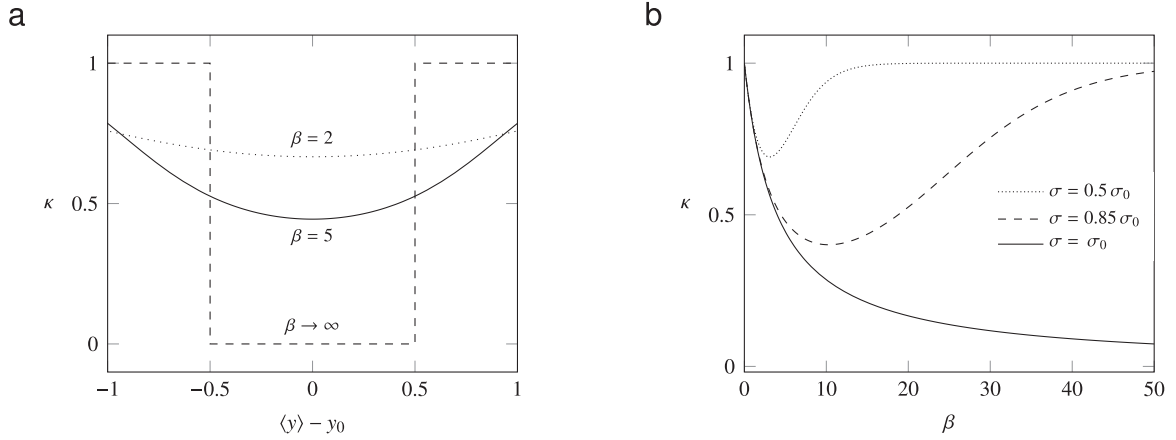
Fig. A.20. Equilibrium stiffness of a single digital switch represented as function of the loading (a), and as function of temperature (b).
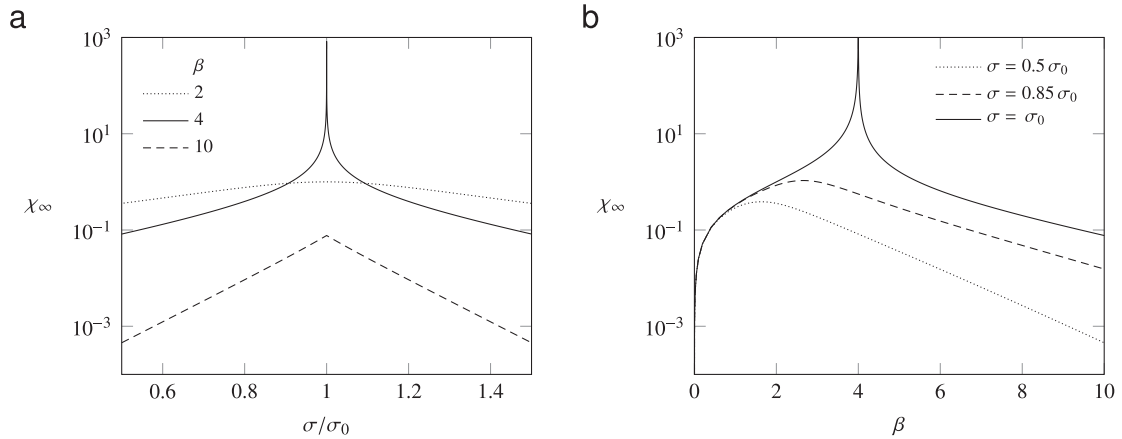

Fig. A.21. Susceptibility of a cluster of bistable elements in the thermodynamic limit as function of the loading (a) and as function of temperature (b).

We define the rescaled susceptibility as $\chi = NX$. In the thermodynamic limit, we have $\langle p \rangle = p_*(\sigma, \beta)$ which gives

$$\chi_\infty(\sigma, \beta) = -\frac{1}{N}\frac{\partial}{\partial \sigma} p_*(\sigma, \beta) = \left\{ [\beta p_*(\sigma, \beta)(1 - p_*(\sigma, \beta))]^{-1} - 1 \right\}^{-1}. \tag{A.3}$$

Expanding near the critical point and keeping $\sigma = \sigma_0$, we obtain $\chi_\infty(\sigma, \beta) \sim -\left[1 - \frac{4}{\beta}\right]^{-1}$, which is the analog of the Curie–Weiss law in ferromagnetism (Balian, 2006). Notice that the susceptibility is proportional to the fluctuations, which take the form $\langle [p - \langle p \rangle]^2 \rangle$. Expansion near $\sigma = \sigma_0$ for $\beta = 4$ leads to $\chi_\infty(\sigma, \beta) \sim 4^{-1/3}[3(\sigma - \sigma_0)]^{-2/3}$.

The parameter dependence of the susceptibility χ_∞ is illustrated in Fig. A.21. In agreement with what we learned from the study of a single switching element (see Fig. A.19) the susceptibility reaches its maximum at $\sigma = \sigma_0$, and converges to 0 at both $\beta \to 0$, and $\beta \to \infty$. The main difference is due to the presence of the phase transition occurring at $\beta = 4$, and resulting in a divergence of susceptibility, which is behind large fluctuations observed in Fig. 10(d).

In Fig. A.22 we show the time dependent variance of the evolving order parameter $p(t)$, obtained from the simulations shown in Fig. 15. The results obtained from both the solution of the master equation [(20), lines] and the direct computation in thermal equilibrium (symbols) are shown. At supercritical temperatures and at the critical point, the equilibrium value fit with the numerical simulations well, which confirms that the selected loading protocol is essentially quasi-static; see Fig. A.22, dotted line. However, for $\beta = 6$, the equilibrium behavior—indicated by the diamond in Fig. A.22—is not recovered by the quasi-static simulations in the bi-stable region; see Fig. A.22, dashed line. Instead, kinetic simulations show two peaks corresponding to the collective transitions observed when the system reaches the boundaries of the bistable domain during either loading or unloading.
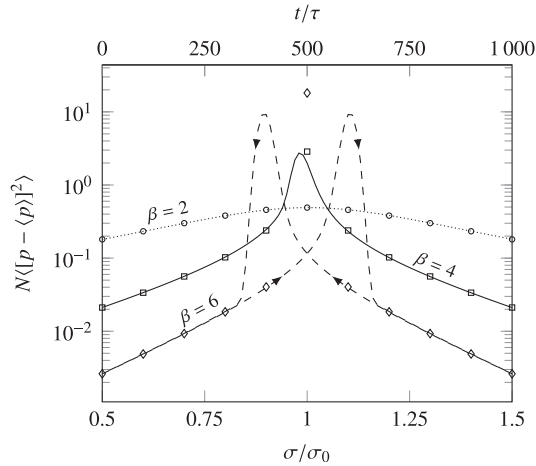
Fig. A.22. Evolution of the variance $\langle (p - \langle p \rangle)^2 \rangle$ obtained from the simulations shown in Fig. 15. Dotted line, $\beta = 2$; solid line, $\beta = 4$; dashed lines, $\beta = 6$. For $\beta = 6$. The symbols on the lines show the variance obtained in thermal equilibrium from the distribution (15) with $\beta = 2$ (circles), $\beta = 4$(squares) and $\beta = 6$ (diamonds).
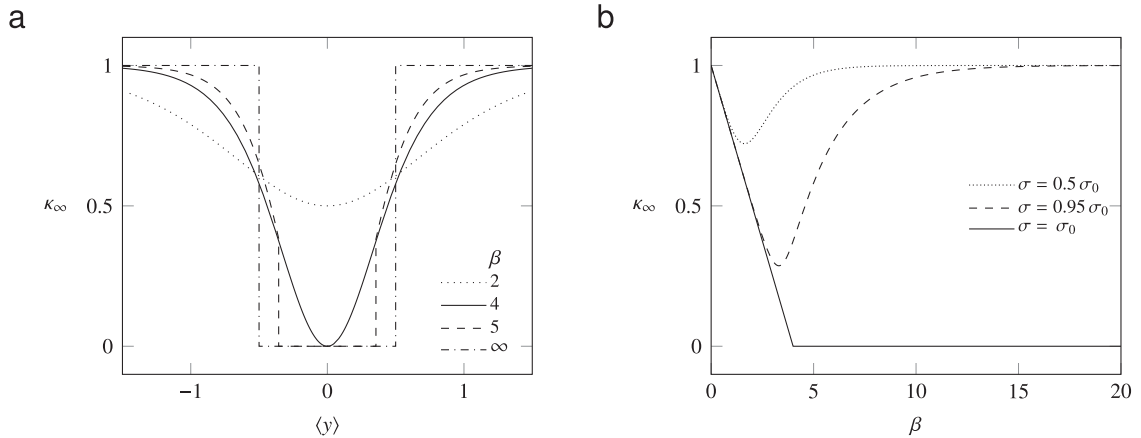

Fig. A.23. Stiffness of a cluster in the thermodynamic limit. (a) As function of the applied load. (b) As function of the temperature.

By computing the derivative of the average displacement (16) with respect to $\Sigma = N\sigma$, we obtain the expression for the equilibrium stiffness

$$K(\sigma, \beta)^{-1} = \frac{1}{N} \frac{\partial}{\partial \sigma} \langle y \rangle (\sigma, \beta) = \beta \langle [y - \langle y \rangle (\sigma, \beta)]^2 \rangle \geq 0,$$

In the hard device case, the stiffness was shown to be sign indefinite (Caruel and Truskinovsky, 2016), while here K is always positive which confirms that the two ensembles are not equivalent. If we denote by $\kappa = K/N$, the stiffness per element, we obtain

$$\kappa(\sigma, \beta) = [1 + \chi(\sigma, \beta)]^{-1},$$

where the susceptibility χ was obtained earlier, see Eq. (A.2). In the thermodynamic limit, $\kappa_\infty(\sigma, \beta) = [1 + \chi_\infty(\sigma, \beta)]^{-1}$ where χ_∞ is given by Eq. (A.3).

The dependence of the stiffness on the applied load and the temperature is illustrated in Fig. A.23. For $\beta < \beta_c$, the behavior is similar to the case of a single switching element, see Fig. A.20: the stiffness is positive, reaches a temperature independent minimum at $\sigma = \sigma_0$ [see (a)] and is equal to 1 at both infinite and zero temperatures [see (b)]. For $\beta > \beta_c$, the two behaviors are rather different. The stiffness of the bundle shows a plateau at a range of temperatures [see Fig. A.23(a)], while in the case of a single element a plateau was obtained only at zero temperature.

Appendix B. Thermal behavior

In addition to the mechanical properties of our "device", it will be of interest to study their thermal properties. First, we present the study the equilibrium thermal behavior of a single switching element. From the partition function (2), we obtain the expression of the equilibrium entropy,

$$s(\sigma, \beta) = -\beta \frac{\partial}{\partial \beta} \log[Z] + \log[Z] = \frac{1}{2} + \frac{1}{2} \log\left[\frac{2\pi}{\beta}\right] + \log\left\{2 \cosh\left[\frac{\beta}{2}(\sigma - \sigma_0)\right]\right\} - \frac{\beta}{2}(\sigma - \sigma_0) \tanh\left[\frac{\beta}{2}(\sigma - \sigma_0)\right].$$

(B.1)

The entropy s is represented as a function of the external load and temperature in Fig. B.24[(a) and (b)]. It reaches a maximum at $\sigma = \sigma_0$, and decreases to a constant (temperature-dependent) value away from this point. The difference between the maximum and the minimum entropy reaches a constant value equal to $\log(2)$ at low temperatures, see Fig. B.24(b).

The dependence of the entropy (B.1) on external load characterizes the heat release $Q(\sigma, \beta) = -(1/\beta)\Delta s(\sigma, \beta)$, where $\Delta s(\sigma, \beta) = s(\sigma, \beta) - s(\sigma_{in}, \beta)$ is the entropy increment starting from the initial state with σ_{in}. The heat release in response to loading from the point $\sigma = \sigma_0$ is represented for different temperatures in Fig. B.24(c). The specific heat c at constant load

$$c(\sigma, \beta) = -\beta \frac{\partial}{\partial \beta} s(\sigma, \beta) = \frac{1}{2} + \left\{\frac{\beta}{2}(\sigma - \sigma_0) \operatorname{sech}\left[\frac{\beta}{2}(\sigma - \sigma_0)\right]\right\}^2,$$

is illustrated in Fig. B.25. We see that specific heat is equal to zero at σ_0 making this state insensitive (robust) to temperature changes. Similarly at large value of the applied force, the mechanical bias of the system dominates the fluctuations, which again makes the system temperature insensitive.

Next we study a bundle of N switching elements. We first define the entropy per element s

$$Ns(\sigma, \beta) = -\beta \frac{\partial}{\partial \beta} \log[Z(\sigma, \beta)] + \log[Z(\sigma, \beta)].$$
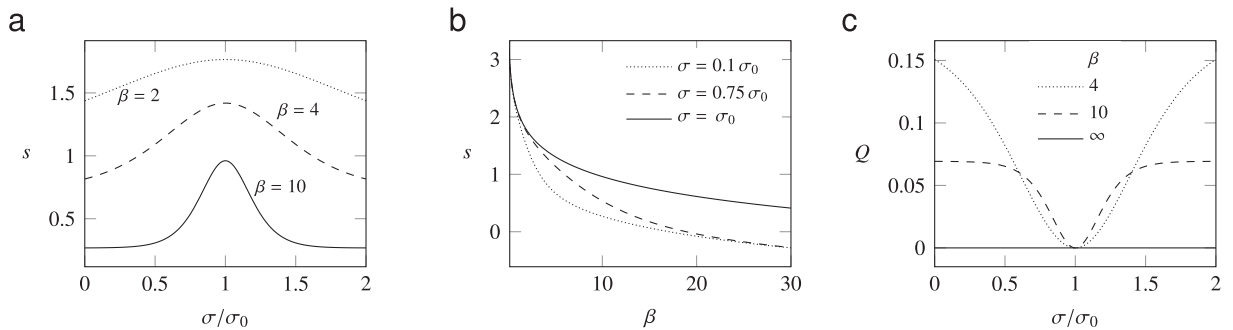

Fig. B.24. Entropy of a single digital switch as function of the external force at different temperatures (a) and as function of temperature for different external forces (b). (b) Heat release in response to a load change from $\sigma = \sigma_0$ for different temperatures.
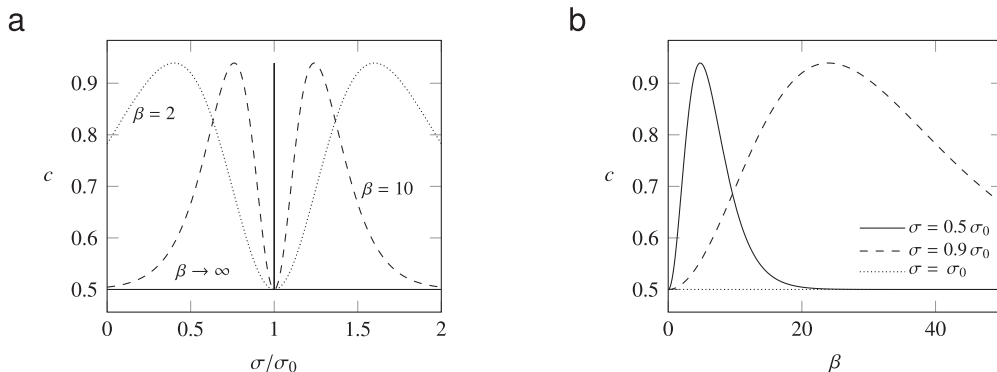

Fig. B.25. Specific heat of a single digital switch as function of the loading (a) and as function of temperature (b).
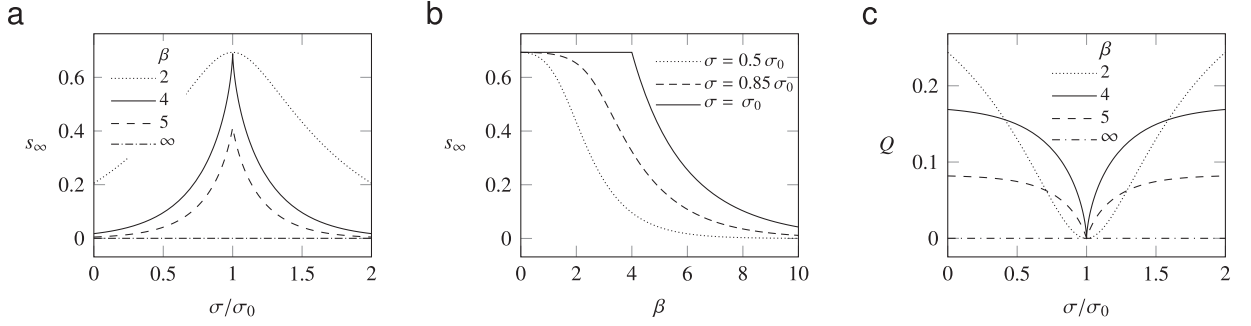
Fig. B.26. Entropy as function of the loading (a) and as function of temperature (b) in the thermodynamic limit. (c) Heat release for different temperatures with the reference state at $\sigma = \sigma_0$.
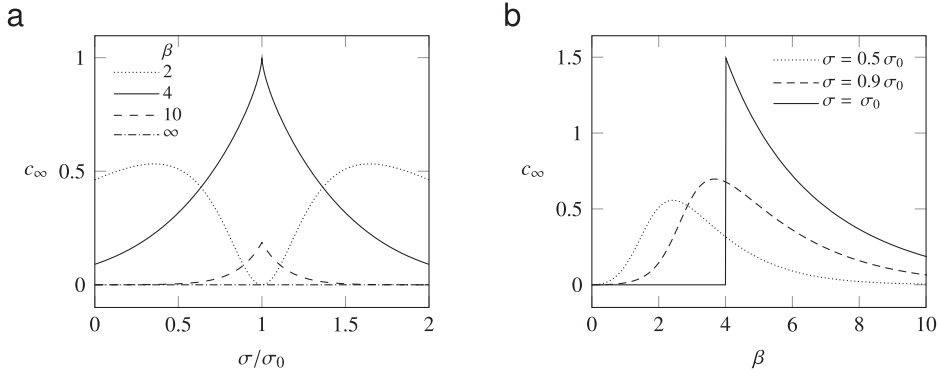

Fig. B.27. Specific heat in the thermodynamic limit as function of the loading (a) and as function of temperature (b).

The function $s(\sigma, \beta)$ can be also written as $s = \beta\langle e \rangle - \beta g$, with the average internal energy is

$$\langle e \rangle(\sigma, \beta) = \sum_p \overline{w}(p; \sigma)\, \overline{\rho}(p; \sigma, \beta) + 1/(2\beta). \tag{B.2}$$

In the thermodynamic limit (B.2) becomes $\langle e \rangle(\sigma, \beta)_\infty(\sigma, \beta) = w[p_*(\sigma, \beta); \sigma, \beta]$, and $s_\infty(\sigma, \beta) = s_\infty[p_*(\sigma, \beta)]$. The dependence of the entropy on temperature and loading is illustrated in Fig. B.26. The entropy is maximized at $\sigma = \sigma_0$, where $\langle p \rangle = 1/2$, and develops a singularity at this point below the critical temperature; see Fig. B.26(a), dashed line. It is always an increasing function of temperature for $\sigma \neq \sigma_0$, except when $\sigma = \sigma_0$, where it is independent of temperature for $\beta < \beta_c$, and is a decreasing function of temperature for $\beta > \beta_c$; see Fig. B.26(a).

The variations of entropy as one goes from one equilibrium state to another can be linked to the heat exchange with the surrounding thermostat : $Q = -\beta^{-1}\Delta s(\sigma, \beta)$, where $\Delta s(\sigma, \beta) = s(\sigma, \beta) - s(\sigma_{\mathrm{in}}, \beta)$. Our Fig. B.26(c) illustrates the heat release starting from the initial equilibrium state at $\sigma_{\mathrm{in}} = \sigma_0$. Below the critical point (dotted line, $\beta = 2$), the heat release is negligible in the vicinity of the initial state as expected from the smooth dependence of the entropy on applied force; see Fig. B.26(a). Above the critical point, the entropy develops a cusp and therefore the heat is released abruptly even for a small external perturbation; see Fig. B.26[(c), solid and dashed lines].

The fact that the capacity of the system to exchange heat with the thermostat is maximal at the critical point can also be seen from the specific heat

$$c(\sigma, \beta) = -\beta \frac{\partial s}{\partial \beta} = \frac{1}{2N} + N\beta^2 \langle [w(p; \sigma, \beta) - \langle w \rangle(\sigma, \beta)]^2 \rangle.$$

In the thermodynamic limit

$$c_\infty(\sigma, \beta) = \frac{1}{\beta}\left\{ \log\left[\frac{p_*}{1 - p_*} \right] \right\}^2 \chi_\infty(\sigma, \beta),$$

where X_∞ is given by Eq. (A.3). Expanding for $\beta > 4$ at $\sigma = \sigma_0$, we obtain $c_\infty(\sigma, \beta) \sim \frac{3}{2}\left[1 - \frac{5}{8}(\beta - 4)\right]$, Similar expansion near $\sigma = \sigma_0$ for $\beta = 4$, leads to $c_\infty(\sigma, \beta) = 1 - 3^{-1/3}(2|\sigma - \sigma_0|)^{2/3}$. These results are illustrated in Fig. B.27.

When the loading is fast at the timescale of heat exchange with the thermostat, the mechanical response becomes adiabatic. To assess the associated temperature variations, we recall that the entropy depends only on $|p - 1/2|$. Therefore, for
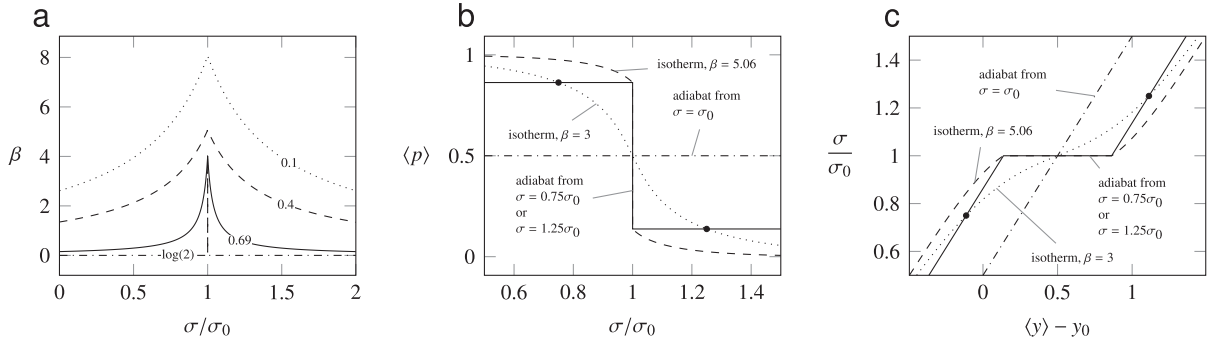
Fig. B.28. Adiabatic response. (a) isoentropes shown for different values of entropy. (b) evolution of $\langle p \rangle$ along adiabats in the thermodynamic limit. Dotdashed, adiabatic response obtained starting from thermal equilibrium at $\sigma = \sigma_0$; Dotted, isotherm corresponding to $\beta = 3$. Solid, adiabatic response obtained when loading the system from the equilibrium state at $\sigma = 0.75\sigma_0$ and $\sigma = 1.25\sigma_0$ with $\beta = 3$ (see the black dots). As the load changes, the value $|p - 1/2|$ is kept constant by a temperature change up to $\beta = 5.06$ at $\sigma = \sigma_0$. The isotherm corresponding to $\beta = 5.06$ is represented by the dashed line. Here $\nu_0 = 1$.

an initial state with entropy s_{in} corresponding to $p = p_{*in}$ we obtain along the adiabat

$$\beta_{AD}(\sigma) = \left[\sigma - \sigma_0 + \text{sign}(\sigma - \sigma_0) \left| \frac{1}{2} - p_{*in} \right| \right]^{-1} \log \left[\frac{\frac{1}{2} + \text{sign}(\sigma - \sigma_0) | \frac{1}{2} - p_{*in} |}{\frac{1}{2} - \text{sign}(\sigma - \sigma_0) | \frac{1}{2} - p_{*in} |} \right]. \tag{B.3}$$

Several typical adiabats of this type (isoentropes) are presented in Fig. B.28 (a). If the system is prepared in an initial equilibrium state at $\sigma > \sigma_0$, and the load is released, the conservation of the initial entropy leads to a decrease in temperature up a finite value of β, but then the temperature rises again as the load continues to decrease for $\sigma < \sigma_0$.

The reason why the temperature drops to a finite value during the unloading becomes clear when we examine Fig. B.28 (b), showing the evolution of $\langle p \rangle$ along the adiabats. Suppose the system is prepared in thermal equilibrium at $\beta = 3$, and $\sigma = 1.25\sigma_0$ [see Fig. B.28(b), black dot where $p_{in} \approx 0.89$], and then the load is dropped to a value below σ_0. First, the temperature decreases as the system has to maintain the initial value $\langle p \rangle = p_{in}$, and this process continues till the applied load reaches the value σ_0. The value of β_{AD}, ensuring that $\langle p \rangle (\sigma_0, \beta_{AD}) = p_{in}$, is about 5.06. The isotherm corresponding to $\beta = 5.06$ is represented by the dashed line in Fig. B.28(b), and we see that the adiabatic trajectory (solid line) intercept the isotherm at the jump point. As the load is decreased further, the temperature starts to increase from the value $\beta = 5.06$ as the system has to maintain the new value of $\langle p \rangle = 1 - p_{in}$.

Appendix C. Boundaries of the bistable domain

The critical points of $\bar{g}_\infty$ are solutions of $\frac{\partial}{\partial p} \bar{g}_\infty = 0$, namely of

$$\sigma - \sigma_0 = p - \frac{1}{2} - \frac{1}{\beta} \ln \left[\frac{p}{1 - p} \right], \tag{C.1}$$

for which the number of solutions depends on the variations of the right hand side. We have,

$$\frac{\partial^2 \bar{g}_\infty}{\partial p^2} = -1 + [\beta p (1 - p)]^{-1}$$

which when $\beta > 4$ is equal to zero for $p = p_+(\beta)$ and $p = p_-(\beta)$ with

$$\begin{align} p_+(\beta) &= (1 + \sqrt{1 - 4\beta^{-1}})/2 \\ p_-(\beta) &= (1 - \sqrt{1 - 4\beta^{-1}})/2. \end{align} \tag{C.2}$$

By inserting these values in Eq. (C.1) we obtain,

$$\begin{align} \sigma_+(\beta) &= \sigma_0 + \frac{1}{2}\sqrt{1 - \frac{4}{\beta}} - \frac{1}{\beta} \log \left[\frac{\sqrt{\beta} + \sqrt{\beta - 4}}{\sqrt{\beta} - \sqrt{\beta - 4}} \right] \\ \sigma_-(\beta) &= \sigma_0 - \frac{1}{2}\sqrt{1 - \frac{4}{\beta}} + \frac{1}{\beta} \log \left[\frac{\sqrt{\beta} + \sqrt{\beta - 4}}{\sqrt{\beta} - \sqrt{\beta - 4}} \right] \end{align} \tag{C.3}$$

Hence we find that the system has 3 critical points when $\sigma_-(\beta) < \sigma < \sigma_+(\beta)$. In the limit $\beta \to \infty$ we obtain that $\sigma_+ = \nu_0 + 1/2$ and to $\sigma_- = \nu_0 - 1/2$, when $\beta \to \infty$, respectively; see Caruel et al. (2015).

References

Achenbach, M., Atanackovic, T., Müller, I., 1986. A model for memory alloys in plane strain. Int. J. Solids Struct. 22 (2), 171–193.

Balian, R., 2006. From Microphysics to Macrophysics. Methods and Applications of Statistical Physics. Springer Science & Business Media.

Barré, J., Mukamel, D., Ruffo, S., 2002. Ensemble Inequivalence in Mean-Field Models of Magnetism. In: Dynamics and Thermodynamics of Systems with Long-Range Interactions. Springer Berlin Heidelberg, Berlin, Heidelberg, pp. 45–67.

Bell, G., 1978. Model for the specific adhesion of cells to cells. Science 200.

Bell, S., Terentjev, E.M., 2017. Focal adhesion kinase: the reversible molecular mechanosensor.. Biophys. J. 112 (11), 2439–2450.

Benichou, I., Givli, S., 2015. Rate dependent response of nanoscale structures having a multiwell energy landscape.. Phys. Rev. Lett. 114 (9), 095504.

Benichou, I., Zhang, Y., Dudko, O.K., Givli, S., 2016. The rate dependent response of a bistable chain at finite temperature. J. Mech. Phys. Solids 95, 44–63.

Bormuth, V., Barral, J., Joanny, J.F., Jülicher, F., Martin, P., 2014. Transduction channels' gating can control friction on vibrating hair-cell bundles in the ear. Proc. Natl. Acad. Sci. U.S.A. 111 (20), 7185–7190.

Bückmann, T., Kadic, M., Schittny, R., Wegener, M., 2015. Mechanical cloak design by direct lattice transformation.. Proc. Natl. Acad. Sci. U.S.A. 112 (16), 4930–4934.

Caruel, M., Allain, J.-M., Truskinovsky, L., 2015. Mechanics of collective unfolding. J. Mech. Phys. Solids 76, 237–259.

Caruel, M., Truskinovsky, L., 2016. Statistical mechanics of the Huxley-Simmons model. Phys. Rev. E 93 (6), 062407.

Cho, H., Weaver, J.C., Pöselt, E., Boyce, M.C., 2016. Engineering the mechanics of heterogeneous soft crystals. Adv. Funct. Mater. 26 (38), 6938–6949.

Desai, R.C., Zwanzig, R., 1978. Statistical mechanics of a nonlinear stochastic model. J. Stat. Phys. 19, 1–24.

Efendiev, Y.R., Truskinovsky, L., 2010. Thermalization of a driven bi-stable FPU chain. Continuum Mech. Therm. 22 (6–8), 679–698.

Flood, A.H., Stoddart, J.F., Steuerman, D.W., Heath, J.R., 2004. Whence molecular electronics? Science 306 (5704), 2055–2056.

Florijn, B., Coulais, C., van Hecke, M., 2014. Programmable mechanical metamaterials.. Phys. Rev. Lett. 113 (17), 175503.

Frenzel, T., Findeisen, C., Kadic, M., Gumbsch, P., Wegener, M., 2016. Tailored buckling microlattices as reusable light-Weight shock absorbers.. Adv. Mater. Weinheim 28 (28), 5865–5870.

Gardiner, C., 2004. Handbook of Stochastic Methods for Physics Chemistry and the Natural Sciences, third ed. Springer.

Haghpanah, B., Salari-Sharif, L., Pourrajab, P., Hopkins, J., Valdevit, L., 2016. Architected materials: multistable shape-Reconfigurable architected materials (adv. mater. 36/2016). Adv. Mater. 28 (36). 8065–8065

Halg, B., 1990. On a micro-electro-mechanical nonvolatile memory cell. IEEE Trans. Electron Dev. 37 (10), 2230–2236.

Harne, R.L., Wang, K.W., 2013. A review of the recent research on vibration energy harvesting via bistable systems. Smart Mater. Struct. 22 (2), 023001.

Harne, R.L., Wu, Z., Wang, K.W., 2016. Designing and harnessing the metastable states of a modular metastructure for programmable mechanical properties adaptation. J. Mech. Des 138 (2), 021402.

Hill, T.L., 1974. Theoretical formalism for the sliding filament model of contraction of striated muscle part i. Prog. Biophys. Molec. Biol. 28, 267–340.

Hill, T.L., 1976. Theoretical formalism for the sliding filament model of contraction of striated muscle part II. Prog. Biophys. Molec. Biol. 29, 105–159.

Howard, J., Hudspeth, A.J., 1988. Compliance of the hair bundle associated with gating of mechanoelectrical transduction channels in the bullfrog's saccular hair cell.. Neuron 1 (3), 189–199.

Huxley, A.F., Simmons, R.M., 1971. Proposed mechanism of force generation in striated muscle. Nature 233, 533–538.

Huxley, A.F., Tideswell, S., 1996. Filament compliance and tension transients in muscle. J. Muscle Re. Cell M. 17, 507–511.

van Kampen, N., 2001. Stochastic Processes in Physics and Chemistry. North-Holland, Amsterdam.

Kometani, K., Shimizu, H., 1975. A study of self-organizing processes of nonlinear stochastic variables. J. Stat. Phys. 13, 473–490.

Lebowitz, J.L., Penrose, O., 1966. Rigorous treatment of the van der waals-Maxwell theory of the liquid-Vapor transition. J. Math. Phys. 7 (1), 98–113.

Li, X., Gao, H., 2016. Mechanical metamaterials: smaller and stronger.. Nat. Mater. 15 (4), 373–374.

Linari, M., Caremani, M., Lombardi, V., 2010. A kinetic model that explains the effect of inorganic phosphate on the mechanics and energetics of isometric contraction of fast skeletal muscle. P. R. Soc. London B Bio. 277 (270), 19–27.

Martin, P., Mehta, A., Hudspeth, A., 2000. Negative hair-bundle stiffness betrays a mechanism for mechanical amplification by the hair cell. Proc. Natl. Acad. Sci. USA 97 (22), 12026–12031.

Nadkarni, N., Arrieta, A.F., Chong, C., Kochmann, D.M., Daraio, C., 2016. Unidirectional transition waves in bistable lattices.. Phys. Rev. Lett. 116 (24), 244501.

Nicolaou, Z.G., Motter, A.E., 2012. Mechanical metamaterials with negative compressibility transitions. Nat. Mater. 11 (7), 608–613.

Offer, G., Ranatunga, K.W., 2016. Reinterpretation of the tension response of muscle to stretches and releases.. Biophys. J. 111 (9), 2000–2010.

Ollier, E., Labeye, P., Revol, F., 1995. Micro-opto mechanical switch integrated on silicon. Electron. Lett. 31 (23), 2003–2005.

Paulose, J., Meeussen, A.S., Vitelli, V., 2015. Selective buckling via states of self-stress in topological metamaterials.. Proc. Natl. Acad. Sci. U.S.A. 112 (25), 7639–7644.

Piazzesi, G., Lombardi, V., 1995. A cross-bridge model that is able to explain mechanical and energetic properties of shortening muscle. Biophys. J. 68 (5), 1966–1979.

Rafsanjani, A., Akbarzadeh, A., Pasini, D., 2015. Snapping mechanical metamaterials under tension. Adv. Mater. 27 (39), 5930.

Receveur, R.A.M., Marxer, C.R., Woering, R., Larik, V.C.M.H., de Rooij, N.F., 2005. Laterally moving bistable MEMS DC switch for biomedical applications. J. Microelectromech. Syst. 14 (5), 1089–1098.

Reconditi, M., Linari, M., Lucii, L., Stewart, A., Sun, Y., Boesecke, P., Narayanan, T., Fischetti, R., Irving, T., Piazzesi, G., Irving, M., Lombardi, V., 2004. The myosin motor in muscle generates a smaller and slower working stroke at higher load. Nature 428 (6982), 578–581.

Shan, S., Kang, S.H., Raney, J.R., Wang, P., Fang, L., Candido, F., Lewis, J.A., Bertoldi, K., 2015. Multistable architected materials for trapping elastic strain energy.. Adv. Mater. Weinheim 27 (29), 4296–4301.

Sheshka, R., Recho, P., Truskinovsky, L., 2016. Rigidity generation by nonthermal fluctuations. Phys. Rev. E 93 (5), 052604–052614.

Shiino, M., 1987. Dynamical behavior of stochastic systems of infinitely many coupled nonlinear oscillators exhibiting phase transitions of mean-field type: H theorem on asymptotic approach to equilibrium and critical slowing down of order-parameter fluctuations.. Phys Rev A Gen Phys 36 (5), 2393–2412.

Smith, D., Geeves, M., Sleep, J., Mijailovich, S., 2008. Towards a unified theory of muscle contraction. 1: foundations. Ann. Biomed. Eng. 36, 1624–1640.

Steuerman, D.W., Tseng, H.R., Peters, A.J., Flood, A.H., Jeppesen, J.O., Nielsen, K.A., Stoddart, J.F., Heath, J.R., 2004. Molecular-mechanical switch-based solid-state electrochromic devices. Angewandte Chemie 116 (47), 6648–6653.

Südhof, T.C., 2013. Neurotransmitter release: the last millisecond in the life of a synaptic vesicle. Neuron 80 (3), 675–690.

Wu, Z., Harne, R., Wang, K., 2016. Exploring a modular adaptive metastructure concept inspired by muscles cross-bridge. J. Intell. Mat. Syst. Struct. 27 (9), 1189–1202.

Wu, Z., Harne, R.L., Wang, K.W., 2014. Muscle-like characteristics with an engineered metastructure. In: ASME 2014 Conference on Smart Materials, Adaptive Structures and Intelligent Systems.

Xin, F., Lu, T., 2016. Tensional acoustomechanical soft metamaterials.. Sci. Rep. 6, 27432.

Zwanzig, R., 1988. Diffusion in a rough potential. PNAS 85 (7), 2029–2030.